

Resummed azimuthal decorrelation and transverse momentum imbalance of dijets at the LHC

Rong-Jun Fu^a, Rudi Rahn^b, Ding Yu Shao^{a,c,d}, Wouter J. Waalewijn^{e,f} and Bin Wu^g

^a*Department of Physics, Center for Field Theory and Particle Physics and Key Laboratory of Nuclear Physics and Ion-beam Application (MOE), Fudan University, Shanghai, 200433, China*

^b*University of Vienna, Faculty of Physics, Boltzmannngasse 5, A-1090 Wien, Austria*

^c*Shanghai Research Center for Theoretical Nuclear Physics, NSFC and Fudan University, Shanghai 200438, China*

^d*Center for High Energy Physics, Peking University, Beijing 100871, China*

^e*Nikhef, Theory Group, Science Park 105, 1098 XG, Amsterdam, The Netherlands*

^f*Institute for Theoretical Physics Amsterdam and Delta Institute for Theoretical Physics, University of Amsterdam, Science Park 904, 1098 XH Amsterdam, The Netherlands*

^g*Instituto Galego de Física de Altas Enerxías IGFAE, Universidade de Santiago de Compostela, E-15782 Galicia-Spain*

E-mail: rjfu23@m.fudan.edu.cn, rudi.rahn@univie.ac.at, dyshao@fudan.edu.cn, w.j.waalewijn@uva.nl, b.wu@cern.ch

ABSTRACT: We present a theoretical study of the azimuthal decorrelation $\delta\phi$ and transverse momentum imbalance q_T in dijet production at the LHC, offering intriguing insights into the dynamics of quantum chromodynamics. We define the jet axes using the recoil-free winner-take-all (WTA) recombination scheme. For the azimuthal decorrelation $\delta\phi$, this axis choice eliminates non-global logarithms (NGLs) entirely. For the transverse momentum imbalance q_T , NGLs emerge specifically in the small jet radius limit ($R \ll 1$). In this regime, the WTA scheme simplifies the theoretical framework by restricting jet radius logarithms to the soft sector. We derive factorization formulae for both observables within soft-collinear effective theory. To address the small- R NGLs in the q_T distribution, we refactorize the soft function into global soft, collinear-soft, and ultra-collinear-soft modes. We perform the resummation of global large logarithms $\ln(\delta\phi)$ and $\ln(q_T/Q)$ up to next-to-next-to-leading logarithmic accuracy. For the q_T distribution, this is combined with a leading-logarithmic resummation of the non-global $\ln R$ terms. We match our predictions to leading fixed-order $\mathcal{O}(\alpha_s^3)$ calculations. We also numerically investigate the structure of the first subleading power corrections. Comparisons with PYTHIA 8 simulations demonstrate that the observables we consider are robust against non-perturbative multi-parton interactions and hadronization effects.

Contents

1	Introduction	2
2	Kinematics	3
2.1	Kinematic analysis	5
3	Factorization and anomalous dimensions	6
3.1	Azimuthal decorrelation	6
3.1.1	Anomalous dimensions for hard, soft, beam and jet functions	8
3.2	Transverse momentum imbalance	10
3.3	Refactorization of q_T -soft function	11
3.3.1	Collinear-soft and ultra-collinear soft functions	13
4	Resummation	15
4.1	Azimuthal decorrelation	15
4.2	Transverse momentum imbalance	15
5	Numerical results	19
5.1	NNLL resummation	20
5.2	Power corrections and NLO matching	21
5.2.1	Power corrections	21
5.2.2	NLO matching	23
6	Conclusions	27
A	NLO global soft functions	28
B	Collinear-soft and ultra-collinear-soft functions up to NNLO	29
B.1	Renormalization and anomalous dimensions in multiplicity space	32
C	Jet radius power corrections from hemisphere soft functions	35
C.1	Integral definition	35
C.2	Boosted hemisphere soft functions	37
C.3	Refactorization of the hemisphere calculation and its power corrections	37
D	Anomalous dimensions	38

1 Introduction

The study of jet production at hadron colliders provides a fundamental test of quantum chromodynamics (QCD) and serves as a crucial tool for probing the structure of the proton. Among the simplest yet most insightful observables in this context are those characterizing the correlations between high transverse momentum objects produced in a back-to-back configuration. For processes such as vector boson plus jet (V +jet) production or inclusive (i.e., without a jet veto) dijet production, momentum conservation in the transverse plane enforces this back-to-back alignment at the Born level. However, soft and collinear radiation induces deviations from this topology, generating imbalances in the transverse momentum q_T or azimuthal angle $\delta\phi$. The azimuthal decorrelation is sensitive to the dynamics of QCD radiation and is of significant experimental interest at the LHC [1–11]. The transverse momentum imbalance is used, for example, in jet calibration [12, 13]. Furthermore, single-spin asymmetries in back-to-back dijet production at polarized proton-proton colliders serve as crucial probes for the three-dimensional tomographic imaging of the proton and the study of quark and gluon transverse-momentum-dependent (TMD) parton distribution functions (PDFs) [14–20]. The consistent extraction of these TMD distributions is complicated by potential factorization-breaking effects [21–30].

Precise theoretical predictions for these observables require the all-order resummation of large logarithms that emerge in the back-to-back limit. However, achieving high logarithmic accuracy for jet observables is notoriously difficult due to the presence of non-global logarithms (NGLs) [31]. These arise from soft radiation that is sensitive to the jet boundary, leading to complex factorization structures [32–36]. Consequently, theoretical predictions for these TMD-like observables using standard jet definitions have traditionally been restricted to next-to-leading logarithmic (NLL) accuracy [37–41], though recent theoretical efforts have begun extending this frontier toward next-to-next-to-leading logarithmic (NNLL) precision [42–44].

In this paper, we study the azimuthal decorrelation $\delta\phi$ and the transverse momentum imbalance q_T in inclusive dijet production. To address the challenge of NGLs, we adopt the winner-take-all (WTA) recombination scheme [45, 46] to define the jet axes. The WTA scheme is *recoil-free*, meaning the direction of the jet axis is insensitive to soft recoil [47, 48]. This property eliminates NGLs from the factorization of the azimuthal decorrelation $\delta\phi$, enabling high-precision resummation, as demonstrated in previous studies of V +jet production [49, 50].

The theoretical framework for q_T is more nuanced. While the WTA scheme removes NGLs from the azimuthal decorrelation, the transverse momentum imbalance retains a sensitivity to NGLs in the small jet radius limit ($R \ll 1$), even under WTA definitions [50]. Building on recent developments in transverse momentum slicing for WTA jets [51], we here investigate the logarithmic structure of the q_T distribution. We show that the WTA scheme allows us to isolate the origin of these NGLs as jet radius logarithms ($\ln R$) within the soft sector. This enables a joint resummation framework within soft-collinear effective theory (SCET) [52–57], where global logarithms $\ln(q_T/p_T)$ are resummed to NNLL accuracy, while the NGLs arising from the interplay between collinear-soft and ultra-collinear-soft modes

are resummed to LL accuracy.

Here we extend the WTA-based resummation framework from V +jet to inclusive dijet production, which involves several non-trivial theoretical advancements: Unlike V +jet processes, the dijet sector is characterized by a large number of partonic channels and non-trivial color structures. This complexity necessitates a more sophisticated treatment of the hard function to describe the scattering process and the soft function to encode wide-angle radiation from both the incoming and outgoing hard partons. Furthermore, the role of linearly polarized gluons differs significantly. While they contribute at next-to-leading order (NLO) for massive vector boson plus jet production [49], their impact in the dijet case only emerges at next-to-next-to-leading order (NNLO) [51].

The resummation structure itself is also modified. For the two-component transverse momentum, the collinear and soft radiation confined within the jet contribute only via the momentum component perpendicular to the beam-jet plane. Additionally, the distinct treatment of soft radiation across the jet boundary introduces NGLs. In the WTA scheme, these are specifically identified as NGLs of the jet radius R . To resum them, we perform a refactorization of the soft function into global soft, collinear-soft, and ultra-collinear-soft modes, and we find their numerical impact to be relatively mild. Finally, we refine the fixed-order matching procedure. While V +jet matching is often complicated by large corrections from similar final states in electroweak sectors [58], the dijet matching presented here provides a robust baseline for high-precision LHC phenomenology.

Our main results include a comprehensive phenomenological study at the LHC. We present NNLL resummed predictions for both $\delta\phi$ and q_T , matched to NLO fixed-order results generated by NLOJET++ [59–61] and analyzed using FASTJET [62]. We discuss the substantial reduction in theoretical uncertainties achieved by the resummation and analyze the impact of non-perturbative effects by comparing our predictions with PYTHIA 8 [63] simulations. We find that both $\delta\phi$ and q_T are robust against hadronization and multi-parton interactions.

The paper is organized as follows. Section 2 introduces the kinematic setup and the definitions of the observables. In section 3, we derive the factorization formulae for $\delta\phi$ and q_T , with a detailed discussion of the small- R refactorization for the q_T soft function. The resummation of large logarithms and the evolution equations needed to accomplish this are presented in section 4. In section 5, we present our numerical results, including uncertainty estimates, matching to fixed order, and comparisons with Monte Carlo simulations. We conclude in section 6.

2 Kinematics

We consider the inclusive dijet production process at hadron colliders,

$$p(P_a) + p(P_b) \rightarrow J(p_1) + J(p_2) + X.$$

Here, $p(P_{a,b})$ denote the incoming protons, $J(p_{1,2})$ are the two leading final-state jets, and X represents unobserved hadronic radiation. At the Born level, this corresponds to a

2 \rightarrow 2 partonic scattering process. Treating all partons as massless, we parameterize their four-momenta in the laboratory frame as

$$p_a^\mu = x_a P_a^\mu = x_a \frac{\sqrt{s}}{2}(1, 0, 0, 1), \quad p_b^\mu = x_b P_b^\mu = x_b \frac{\sqrt{s}}{2}(1, 0, 0, -1), \quad (2.1)$$

$$p_1^\mu = p_T(\cosh \eta_1, 1, 0, \sinh \eta_1), \quad p_2^\mu = p_T(\cosh \eta_2, -1, 0, \sinh \eta_2), \quad (2.2)$$

where $s \equiv (P_a + P_b)^2$, and p_T and $\eta_{1,2}$ are the transverse momentum and rapidities of the outgoing partons, which are back-to-back in the transverse plane. The partonic momentum fractions $x_{a,b}$ are fixed by

$$x_a = \frac{p_T}{\sqrt{s}}(e^{\eta_1} + e^{\eta_2}), \quad x_b = \frac{p_T}{\sqrt{s}}(e^{-\eta_1} + e^{-\eta_2}). \quad (2.3)$$

The partonic Mandelstam variables are then given by

$$\hat{s} = (p_a + p_b)^2 = x_a x_b s = 2p_T^2[1 + \cosh(\eta_1 - \eta_2)], \quad (2.4)$$

$$\hat{t} = (p_a - p_1)^2 = -p_T^2(1 + e^{\eta_2 - \eta_1}), \quad (2.5)$$

$$\hat{u} = (p_a - p_2)^2 = -p_T^2(1 + e^{\eta_1 - \eta_2}). \quad (2.6)$$

Beyond the Born approximation, jets are clustered using the anti- k_T algorithm with the standard E -scheme. This work focuses on the back-to-back kinematic regime, where the total dijet transverse momentum $q_T \rightarrow 0$. In this limit, the cross section is sensitive to large logarithms, such as $\ln(q_T/Q)$ where $Q \sim p_T$, which spoil the convergence of fixed-order perturbation theory and require resummation.

A known complication of all-order resummation in such scenarios is the presence of NGLs. To circumvent this issue, we define our observables using the winner-take-all (WTA) recombination scheme, rather than the standard E -scheme. The WTA scheme is recoil-free and is known to eliminate NGLs from the factorization. Explicitly, we measure the dijet transverse momentum imbalance \vec{q}_T and the azimuthal acoplanarity $\delta\phi$ defined by

$$\vec{q}_T \equiv \vec{p}_{1,T}^{\text{WTA}} + \vec{p}_{2,T}^{\text{WTA}}, \quad \delta\phi \equiv |\pi - |\phi_1^{\text{WTA}} - \phi_2^{\text{WTA}}||. \quad (2.7)$$

Here, $\vec{p}_{i,T}^{\text{WTA}}$ and ϕ_i^{WTA} are the transverse momentum and azimuthal angle of the jet axis defined by the WTA scheme. It is important to note that these kinematic quantities are distinct from the transverse momentum $\vec{p}_{i,T}$ and azimuthal angle ϕ_i that would be obtained using the standard E -scheme. While the change in transverse momentum and rapidity of the individual jets due to the scheme choice is rather small, the effect on \vec{q}_T and $\delta\phi$ is not small because these observables involve large cancellations between the two almost back-to-back jets.

Even with this simplification, the resummations for q_T and $\delta\phi$ remain distinct. As demonstrated in ref. [51], the q_T and $\delta\phi$ distributions possess different factorization structures. In section 3, we will derive the factorization and resummation formulae for both of these observables.

2.1 Kinematic analysis

According to the WTA- p_T scheme defined in the transverse plane perpendicular to the beam axis, we can rewrite the observable \vec{q}_T in a more explicit form as

$$\begin{aligned}\vec{q}_T &\equiv \vec{p}_{1,T}^{\text{WTA}} + \vec{p}_{2,T}^{\text{WTA}} \\ &= \left(\sum_{k \in \text{jet-1}} p_{k,T} \right) \vec{n}_{W_1,T} + \left(\sum_{k \in \text{jet-2}} p_{k,T} \right) \vec{n}_{W_2,T},\end{aligned}\quad (2.8)$$

where $\vec{n}_{W_i,T}$ denotes the direction of the WTA axis of jet- i ($i = 1, 2$). Here, we use $\sum_{k \in \text{jet}} p_{k,T}$ to represent the scalar sum of the transverse momentum of all the collinear partons inside the jet. The soft radiation inside the jet is power-suppressed compared with the collinear partons. Utilizing momentum conservation

$$\sum_{k \in \text{jet-1}} \vec{p}_{k,T} + \sum_{k \in \text{jet-2}} \vec{p}_{k,T} + \vec{p}_{a,T} + \vec{p}_{b,T} + \vec{p}_{s,T} = 0, \quad (2.9)$$

we obtain

$$\begin{aligned}\vec{q}_T &= \sum_{k \in \text{jet-1}} (p_{k,T} \vec{n}_{W_1,T} - \vec{p}_{k,T}) + \sum_{k \in \text{jet-2}} (p_{k,T} \vec{n}_{W_2,T} - \vec{p}_{k,T}) - \vec{p}_{a,T} - \vec{p}_{b,T} - \vec{p}_{s,T} \\ &= - \sum_{k \in \text{jet-1}} \vec{p}_{k,\perp}^{(1)} - \sum_{k \in \text{jet-2}} \vec{p}_{k,\perp}^{(2)} - \vec{p}_{a,T} - \vec{p}_{b,T} - \vec{p}_{s,T},\end{aligned}\quad (2.10)$$

where the reconstructed collinear transverse momentum $\vec{p}_{k,\perp}^{(i)}$ ($i = 1, 2$) is defined as

$$\vec{p}_{k,\perp}^{(i)} \equiv \vec{p}_{k,T} - p_{k,T} \vec{n}_{W_i,T}, \quad k \in \text{jet-}i. \quad (2.11)$$

Since $\vec{p}_{k,T}$ is collinear to the jet axis, one has

$$\vec{p}_{k,\perp}^{(i)} \cdot \vec{n}_{W_i,T} = 0 + \mathcal{O}\left(p_{k,T} (\phi_k - \phi_i^{\text{WTA}})^2\right) \quad (2.12)$$

for collinear emissions in jet- i , with ϕ_k the emission's azimuthal orientation. Eq. (2.12) implies that at leading power $\vec{p}_{k,\perp}^{(i)}$ can be treated as perpendicular to the jet and the beam axes, which motivates the subscript \perp . The above derivation is true for $pp \rightarrow N$ jets. Furthermore, when we consider the $pp \rightarrow$ dijet process in a reference frame where the scattering plane lies in the zx -plane at Born level, we find that the transverse momentum of collinear radiation inside the jet is dominated by its y -component. In contrast, collinear radiation along the beam directions and soft radiation exhibit a full two-dimensional transverse-momentum dependence, as shown in eq. (2.10).

Furthermore, if we focus from the outset on the q_y observable (or equivalently, $\delta\phi$)¹, we can directly formulate the factorization expressions in the one-dimensional Fourier-conjugate space associated with b_y , as shown in eq. (3.3).

¹Note that in refs. [41, 50, 51] we used a different convention, using q_x instead of q_y for the component corresponding to $\delta\phi$.

3 Factorization and anomalous dimensions

In this section, we present the TMD factorization structures for the distributions of the azimuthal decorrelation $\delta\phi$ and the transverse momentum imbalance q_T , respectively. We also summarize the anomalous dimensions required for the resummation.

In this paper, we employ the light-cone decomposition with respect to the directions $n_i = (1, \vec{n}_i)$ and $\bar{n}_i = (1, -\vec{n}_i)$, where $|\vec{n}_i| = 1$. An arbitrary momentum p^μ is decomposed as

$$p^\mu = (n_i \cdot p) \frac{\bar{n}_i^\mu}{2} + (\bar{n}_i \cdot p) \frac{n_i^\mu}{2} + p_\perp^\mu \equiv (n_i \cdot p, \bar{n}_i \cdot p, p_\perp^\mu)_{n_i \bar{n}_i}. \quad (3.1)$$

We further define the light-cone components using \pm superscripts as $p^+ \equiv n_i \cdot p$ and $p^- \equiv \bar{n}_i \cdot p$.

3.1 Azimuthal decorrelation

In the back-to-back limit ($\delta\phi \ll 1$), the modes in SCET contributing to the dijet cross section are characterized by the scaling parameter $\lambda \sim \delta\phi$. Explicitly, the momenta scale can be expressed as

- **hard:** $p_h^\mu \sim p_T(1, 1, 1)$,
- $n_{a,b}$ -**collinear:** $p_c^\mu \sim p_T(\lambda^2, 1, \lambda)_{n_i \bar{n}_i}$,
- **soft:** $p_s^\mu \sim p_T(\lambda, \lambda, \lambda)$,
- $n_{1,2}$ -**collinear:** $p_c^\mu \sim p_T(\lambda^2, 1, \lambda)_{n_i \bar{n}_i}$.

Since soft and collinear modes share the same virtuality, rapidity divergences arise in both sectors. These divergences cancel among the corresponding soft, beam and jet functions within the factorization theorem and can be systematically regulated and resummed through frameworks such as the Collins–Soper–Sterman (CSS) formalism [64, 65], the collinear anomaly approach [66, 67], or the rapidity renormalization group (RRG) [68, 69]. In this work, we employ the RRG framework for the subsequent factorization and resummation.

As illustrated in figure 1, in the limit $\delta\phi \rightarrow 0$, the azimuthal deviation is linearly related to the transverse momentum component q_y via

$$\delta\phi \approx \frac{q_y}{p_T}, \quad (3.2)$$

since $q_y = p_T \sin(\delta\phi)$. Consequently, the differential cross section for small $\delta\phi$ factorizes as

$$\begin{aligned} \frac{d^4\sigma}{d\eta_1 d\eta_2 dp_T dq_y} &= \sum_{ijkl} \frac{x_a x_b}{16\pi \hat{s}^2} \frac{2p_T}{1 + \delta_{k\ell}} \mathcal{H}_{ij \rightarrow k\ell, JI}(p_T, \eta_1 - \eta_2, \mu) \\ &\times \int_{-\infty}^{\infty} \frac{db_y}{2\pi} e^{ib_y q_y} \mathcal{S}_{ijkl, IJ}(b_y, \eta_1, \eta_2, \mu, \nu) \mathcal{J}_k(b_y, \omega_1, \mu, \nu) \mathcal{J}_\ell(b_y, \omega_2, \mu, \nu) \end{aligned}$$

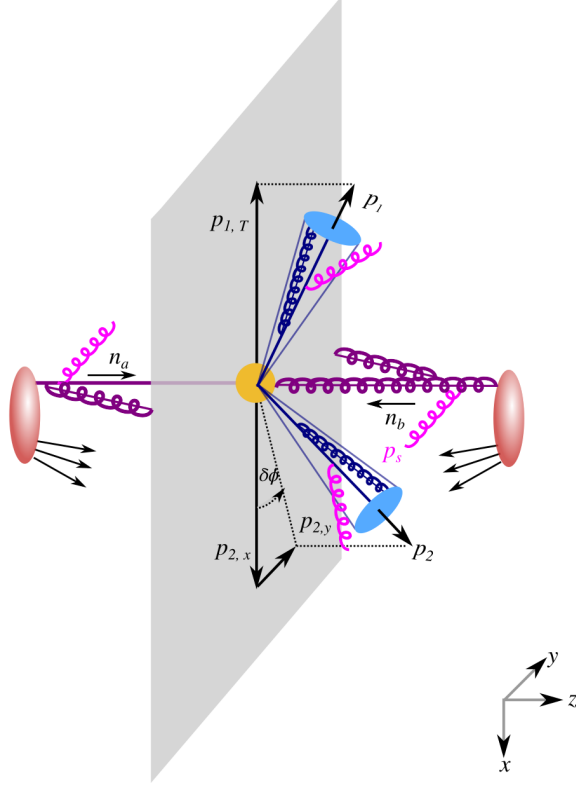


Figure 1: Kinematics of the $pp \rightarrow$ dijet process in the transverse plane. For simplicity, the x -axis is aligned with the first jet, such that $\delta\phi$ corresponds to $q_y = p_{2,y}$. For the factorization theorem, it is more natural to consider a reference frame where the x -axis lies along the direction of the two back-to-back partons that initiate the jets. In this frame, the jet functions encode the offset between these parton directions and the jet axes, while the soft and beam functions capture the recoil induced by soft and initial-state collinear radiation. This choice of frame does not alter the factorization structure.

$$\times B_{i/p}(x_a, b_y, \omega_a, \mu, \nu) B_{j/p}(x_b, b_y, \omega_b, \mu, \nu), \quad (3.3)$$

where ω_i is given by

$$\omega_i = \bar{n}_i \cdot p_i = \begin{cases} x_i \sqrt{s}, & i = a, b \\ 2p_T \cosh \eta_i, & i = 1, 2 \end{cases}.$$

Here, the indices i, j, k, ℓ denote parton flavors, while the symmetry factor $1/(1 + \delta_{k\ell})$ accounts for identical final-state partons. The boldface notation indicates that the hard (\mathcal{H}) and soft (\mathcal{S}) functions are operators in color space, with subscripts I, J representing color indices in the relevant representation. We note that the standard spin and color averaging factors are absorbed into the definition of the hard function [70].

The beam functions $B_{i/p}(x_a, b_y, \omega_a, \mu, \nu)$ encode the initial-state collinear dynamics, describing the radiation emitted by partons extracted from the incoming hadrons prior to the hard interaction. By incorporating transverse recoil effects, they effectively replace the standard parton distribution functions (PDFs) in the regime of small transverse momen-

tum. In the perturbative regime, these beam functions can be matched onto the standard collinear PDFs via an operator product expansion (OPE) as [65, 69, 71]

$$B_{i/p}(x, b_y, \omega, \mu, \nu) = \sum_j \int_x^1 \frac{dx'}{x'} \mathcal{I}_{ij} \left(\frac{x}{x'}, b_y, \omega, \mu, \nu \right) f_j(x', \mu) [1 + \mathcal{O}(\Lambda_{\text{QCD}}^2 b_T^2)]. \quad (3.4)$$

The perturbative matching coefficients \mathcal{I}_{ij} are currently known up to three-loop order [72–74], while the linearly polarized contributions have been determined at two-loop order [75].

Complementarily, the jet functions capture the final-state collinear physics, governing the evolution and fragmentation of energetic partons into the observed jets. In this work, we employ the one-loop jet functions calculated in the WTA recombination scheme [49, 50, 76, 77]. We assume throughout this paper that $\delta\phi, q_T/p_T \ll R$, in which case the jet functions become independent of the jet radius R [76].

Regarding the spin structure of these sectors, we note that linearly polarized gluons can, in principle, participate in the scattering process. However, their effects are absent at the NLO accuracy of our current study, because the hard scattering only involves massless partons.

3.1.1 Anomalous dimensions for hard, soft, beam and jet functions

The massless hard functions are calculated to NNLO for $pp \rightarrow$ dijet process in ref. [70]. The hard function satisfies the following RG equation,

$$\frac{d}{d \ln \mu} \mathcal{H}_{ij \rightarrow k\ell} = \Gamma_{H_{ij \rightarrow k\ell}} \mathcal{H}_{ij \rightarrow k\ell} + \mathcal{H}_{ij \rightarrow k\ell} \Gamma_{H_{ij \rightarrow k\ell}}^\dagger, \quad (3.5)$$

where the anomalous dimension takes the form [70, 78]

$$\begin{aligned} \Gamma_{H_{ij \rightarrow k\ell}} &= \sum_{i < j} \mathbf{T}_i \cdot \mathbf{T}_j \gamma_{\text{cusp}}(\alpha_s) \ln \frac{\mu^2}{-\hat{s}_{ij} - i0} + \gamma_H(\alpha_s) + \mathcal{O}(\alpha_s^3) \\ &= \left[\frac{C_H}{2} \gamma_{\text{cusp}}(\alpha_s) \left(\ln \frac{\hat{s}}{\mu^2} - i\pi \right) + \gamma_H(\alpha_s) \right] \mathbf{1} + \gamma_{\text{cusp}}(\alpha_s) \mathbf{M}_{ij \rightarrow k\ell} + \mathcal{O}(\alpha_s^3), \end{aligned} \quad (3.6)$$

with $C_H = n_q C_F + n_g C_A$ and $\gamma_H = n_q \gamma^q + n_g \gamma^g$. Here n_q and n_g indicate the number of quarks and gluons, respectively. In massless scattering, the partonic Mandelstam invariants are defined as $\hat{s}_{ij} = 2\sigma_{ij} p_i \cdot p_j$ ($i \neq j$), where $\sigma_{ij} = 1$ if both momenta are incoming or outgoing, and $\sigma_{ij} = -1$ otherwise. $\mathbf{M}_{ij \rightarrow k\ell}$ is a non-diagonal color matrix defined by the Catani–Seymour color insertion operators \mathbf{T}_i [79] and a kinematic parameter $r = -\hat{t}/\hat{s}$,

$$\begin{aligned} \mathbf{M}_{ij \rightarrow k\ell} &= -(\ln r + i\pi) (\mathbf{T}_1 \cdot \mathbf{T}_3 + \mathbf{T}_2 \cdot \mathbf{T}_4 + \mathbf{T}_1 \cdot \mathbf{T}_4 + \mathbf{T}_2 \cdot \mathbf{T}_3) \\ &\quad + \ln \frac{r}{1-r} (\mathbf{T}_1 \cdot \mathbf{T}_4 + \mathbf{T}_2 \cdot \mathbf{T}_3). \end{aligned} \quad (3.7)$$

Analogous to the hard functions, the soft functions satisfy RG equations in color space that mix color structures under the RG evolution,

$$\frac{d}{d \ln \mu} \mathbf{S}_{ijkl} = (\mathbf{\Gamma}_\mu^{S_{ijkl}})^\dagger \mathbf{S}_{ijkl} + \mathbf{S}_{ijkl} \mathbf{\Gamma}_\mu^{S_{ijkl}}, \quad (3.8)$$

where the anomalous dimension reads [80–84]

$$\Gamma_\mu^{S_{ijkl}} = \sum_{i < j} \mathbf{T}_i \cdot \mathbf{T}_j \gamma_{\text{cusp}}(\alpha_s) \ln \frac{-\sigma_{ij} \nu^2 n_i \cdot n_j - i0}{2\mu^2} - \frac{C_H}{2} \gamma^s(\alpha_s) \mathbf{1} + \mathcal{O}(\alpha_s^3). \quad (3.9)$$

However, after utilizing color conservation, the rapidity divergence in the soft function is found to be proportional to the Casimir operators. This result is consistent with the cancellation of rapidity divergences between the soft function and the color-diagonal beam and jet functions. Therefore, the RRG equations of soft functions do not include any mixture of different color information,

$$\frac{d}{d \ln \nu} \mathbf{S}_{ijkl} = \Gamma_\nu^{S_{ijkl}} \mathbf{S}_{ijkl}, \quad (3.10)$$

where

$$\Gamma_\nu^{S_{ijkl}} = -C_H \gamma_{\text{cusp}}(\alpha_s) L_b - \left(\frac{\alpha_s}{4\pi}\right)^2 C_H \left(\frac{\beta_0}{2} \gamma_0^{\text{cusp}} L_b^2 - \frac{\gamma_1^\nu}{2}\right) + \mathcal{O}(\alpha_s^3), \quad (3.11)$$

and the first term contains both an α_s and α_s^2 contribution, with $L_b = \ln(\mu^2 b^2 / b_0^2)$ and $b_0 = 2e^{-\gamma_E}$.

By investigating the anomalous dimensions of beam functions and jet functions, we find that for $\mathcal{F}_i \in \{B_i, \mathcal{J}_i\}$, their RG equations are as follows,

$$\frac{d}{d \ln \mu} \mathcal{F}_i(b, \mu, \nu) = \Gamma_\mu^{\mathcal{F}_i}(b, \nu) \mathcal{F}_i(b, \mu, \nu), \quad (3.12)$$

where

$$\Gamma_\mu^{\mathcal{F}_i}(b, \nu) = 2C_i \gamma_{\text{cusp}}(\alpha_s) \ln \frac{\nu}{\omega_i} + \gamma^{\mathcal{F}_i}. \quad (3.13)$$

RRG equations for \mathcal{F}_i take the form

$$\frac{d}{d \ln \nu} \mathcal{F}_i(b, \mu, \nu) = \Gamma_\nu^i(b, \mu) \mathcal{F}_i(b, \mu, \nu), \quad (3.14)$$

where

$$\Gamma_\nu^i(b, \mu) = C_i \gamma_{\text{cusp}} L_b + \left(\frac{\alpha_s}{4\pi}\right)^2 C_i \left(\frac{\beta_0}{2} \gamma_0^{\text{cusp}} L_b^2 - \frac{\gamma_1^\nu}{2}\right) + \mathcal{O}(\alpha_s^3). \quad (3.15)$$

Explicit expressions for the perturbative expansions of the non-cusp anomalous dimensions γ^q , γ^g , γ^s , $\gamma^{\mathcal{F}_i}$ and the non-cusp rapidity anomalous dimension γ^ν are provided in appendix D.

As a non-trivial check of our theoretical framework, we have verified the RRG consistency

$$\Gamma_\nu^{S_{ijkl}} + \sum_{i=a,b,1,2} \Gamma_\nu^i = 0, \quad (3.16)$$

and the RG consistency

$$\frac{d}{d \ln \mu} [\text{tr}(\mathcal{H}\mathcal{S}) B_a B_b \mathcal{J}_1 \mathcal{J}_2] = 0. \quad (3.17)$$

3.2 Transverse momentum imbalance

In SCET, the kinematic modes relevant for the q_T distribution are given by

- **hard:** $p_h^\mu \sim p_T(1, 1, 1)$,
- $n_{a,b}$ -**collinear:** $p_{c_i}^\mu \sim (q_T^2/p_T, p_T, q_T)_{n_i \bar{n}_i}$,
- $n_{1,2}$ -**collinear:** $p_{c_i}^\mu \sim (q_y^2/p_T, p_T, q_y)_{n_i \bar{n}_i}$,

where the soft modes are not shown here, as their structure is more intricate and requires further refactorization in the small- R limit.

The factorization formula for the q_T distribution is written as

$$\begin{aligned}
\frac{d^4\sigma}{d\eta_1 d\eta_2 dp_T dq_T} &= \sum_{ijkl} \frac{x_a x_b}{16\pi \hat{s}^2} \frac{2p_T}{1 + \delta_{kl}} q_T \int_0^{2\pi} d\phi_q \int d\vec{k}_{s,T} d\vec{k}_{a,T} d\vec{k}_{b,T} dk_{1,y} dk_{2,y} \quad (3.18) \\
&\times \text{tr} \left[\mathcal{H}_{ij \rightarrow kl}(p_T, \eta_1 - \eta_2, \mu) \mathcal{S}_{ijkl}(\vec{k}_{s,T}, \eta_1, \eta_2, R, \mu, \nu) \right] \\
&\times \mathcal{J}_k(k_{1,y}, \omega_1, \mu, \nu) \mathcal{J}_\ell(k_{2,y}, \omega_2, \mu, \nu) \\
&\times B_{i/p}(x_a, \vec{k}_{a,T}, \omega_a, \mu, \nu) B_{j/p}(x_b, \vec{k}_{b,T}, \omega_b, \mu, \nu) \\
&\times \delta(q_y + k_{s,y} + k_{a,y} + k_{b,y} + k_{1,y} + k_{2,y}) \delta(q_x + k_{s,x} + k_{a,x} + k_{b,x}).
\end{aligned}$$

The soft function in eq. (3.18) differs from the q_y soft function. In particular, it distinguishes radiation inside and outside jets and thus depends on the jet radius.

We can apply a Fourier transform to the factorization ingredients in eq. (3.18), converting the convolution of different $\vec{k}_{i,T}$ into a product in \vec{b}_T space,

$$\mathcal{S}_{ijkl}(\vec{b}_T, \eta_1, \eta_2, R, \mu, \nu) = \int_{-\infty}^{\infty} d\vec{k}_{s,T} e^{i\vec{k}_{s,T} \cdot \vec{b}_T} \mathcal{S}_{ijkl}(\vec{k}_{s,T}, \eta_1, \eta_2, R, \mu, \nu), \quad (3.19)$$

$$B_{i/p}(x_a, \vec{b}_T, \omega_a, \mu, \nu) = \int_{-\infty}^{\infty} d\vec{k}_{a,T} e^{i\vec{k}_{a,T} \cdot \vec{b}_T} B_{i/p}(x_a, \vec{k}_{a,T}, \omega_a, \mu, \nu), \quad (3.20)$$

$$J_k(b_y, \omega_1, \mu, \nu) = \int_{-\infty}^{\infty} dk_{1,y} e^{ik_{1,y} b_y} J_k(k_{1,y}, \omega_1, \mu, \nu). \quad (3.21)$$

The hard, jet, and beam functions entering here are defined in the same way as in the $\delta\phi$ distribution. The only modification arises in the TMD beam functions: here they depend on the full transverse momentum of the initial collinear modes rather than solely on the y -component. Fortunately, since TMD beam functions are isotropic in the transverse plane, the replacement $b_y \rightarrow b_T$ in $B_{i/p}(x_a, b_y, \omega_a, \mu, \nu)$ suffices. The most significant difference between the factorization formulas for the $\delta\phi$ and q_T distributions lies in the soft function. The soft function $\mathcal{S}_{ijkl}(\vec{b}_T, \eta_1, \eta_2, R, \mu, \nu)$ describes the recoil from soft radiation emitted by the beams and jets on the two WTA axes. We will elaborate on its detailed refactorization structure in the small- R limit in section 3.3.

The factorization formula for the q_T spectrum, written in impact parameter space, is given by

$$\begin{aligned} \frac{d^4\sigma}{d\eta_1 d\eta_2 dp_T dq_T} &= \sum_{ijkl} \frac{x_a x_b}{16\pi\hat{s}^2} \frac{2p_T}{1 + \delta_{kl}} \mathcal{H}_{ij \rightarrow kl, JI}(p_T, \eta_1 - \eta_2, \mu) q_T \int_0^{2\pi} d\phi_q \int \frac{d^2\vec{b}_T}{(2\pi)^2} e^{i\vec{q}_T \cdot \vec{b}_T} \\ &\times \mathcal{S}_{ijkl, IJ}(\vec{b}_T, \eta_1, \eta_2, R, \mu, \nu) \mathcal{J}_k(b_y, \omega_1, \mu, \nu) \mathcal{J}_\ell(b_y, \omega_2, \mu, \nu) \\ &\times B_{i/p}(x_a, \omega_a, b_T, \mu, \nu) B_{j/p}(x_b, \omega_b, b_T, \mu, \nu). \end{aligned} \quad (3.22)$$

3.3 Refactorization of q_T -soft function

In the small- R limit², the TMD soft function can be refactorized into the product of a global TMD soft function, which is independent of the jet definition, and the functions, S_i , describing soft radiation near the jet boundaries. The relevant modes for this factorization are

- **soft:** $p_s^\mu \sim q_T (1, 1, 1)$,
- **n_i -collinear-soft:** $p_{cs}^\mu \sim |q_y|/R (R^2, 1, R)_{n_i \bar{n}_i}$,
- **n_i -ultra-collinear-soft:** $p_{ucs}^\mu \sim q_T (R^2, 1, R)_{n_i \bar{n}_i}$,

with $i = 1$ or 2 . The soft modes share the same virtuality, q_T^2 , as the beam functions, while the collinear-soft modes and jet functions have the same virtuality, q_y^2 , as illustrated in figure 2. We employ the RRG framework to address the pairwise cancellation of rapidity divergences between modes with the same virtuality.

Based on this mode analysis, we factorize the small- R q_T -soft function into

$$\begin{aligned} \mathcal{S}_{ijkl}(\vec{b}_T, R, \phi_1, \phi_2, \eta_1, \eta_2, \mu, \nu) &= \\ \mathcal{S}_{ijkl}^{\text{global}}(\vec{b}_T, \phi_1, \phi_2, \eta_1, \eta_2, \mu, \nu) S_k(\vec{b}_T, \phi_1, \eta_1, R, \mu, \nu) S_\ell(\vec{b}_T, \phi_2, \eta_2, R, \mu, \nu), \end{aligned} \quad (3.23)$$

where the directions n_i are here specified by their rapidity η_i and azimuthal angle ϕ_i . We choose our coordinates such that the azimuthal angle $\phi_1 = 0$ for the final-state parton 1 and $\phi_2 = \pi$ for the final-state parton 2. For brevity, we will suppress this azimuthal dependence in the arguments of the soft functions from here on. The global soft function $\mathcal{S}_{ijkl}^{\text{global}}$ encodes soft radiation from both the incoming beams and the outgoing jets and is independent of the jet definition details. It depends on the jet directions, as the corresponding Wilson lines source soft radiation, but only the total transverse momentum of the global soft radiation is probed through the q_T measurement.

The functions S_i encode the contributions from the n_i -collinear-soft and n_i -ultra-collinear-soft modes. Consequently, S_i is not a single scale function and requires further refactorization. This function describes soft emissions near the jet boundary, which are subject to NGLs beginning at NNLO. To simplify the discussion that follows, we use a

²Note that this does not contradict the assumptions made for the jet function, as the two cases are compatible in the intermediate regime $q_T/p_T \ll R \ll 1$.

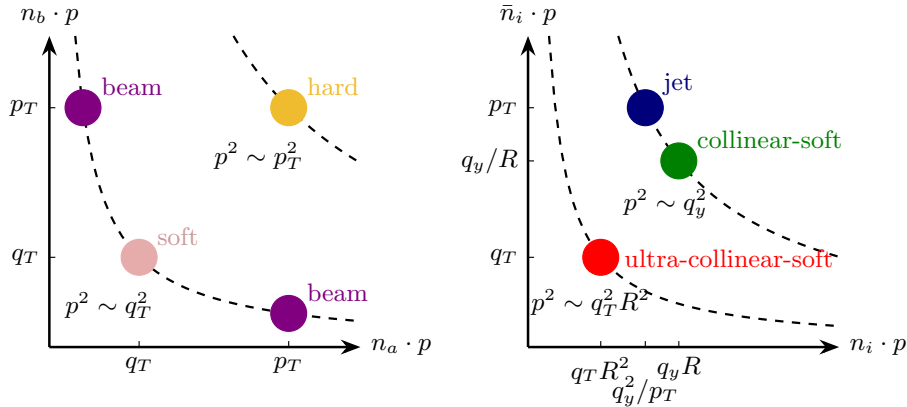


Figure 2: Schematic representation of the relevant modes in the q_T factorization for $pp \rightarrow$ dijets in the small- R limit. **Left:** Standard modes (hard, beam, and soft), where the soft mode represents the global soft function. **Right:** Modes required in the small- R limit, showing the separation of the standard collinear sector into jet, collinear-soft, and ultra-collinear-soft modes. Here $n_i = n_1$ or n_2 .

single leg index $i \in \{1, 2\}$ to denote both the flavor index (k or ℓ) and the corresponding kinematic index (1 or 2).

Inside the jet cone, only the y -component of the soft radiation is measured, whereas outside the jet cone, the full transverse momentum is observed. In the small- R limit, the out-of-cone region technically occupies nearly the entire phase space. However, as demonstrated by the method-of-regions analysis in ref. [51], the wide-angle soft radiation away from the jet boundary is scaleless; the real and virtual corrections cancel exactly, resulting in a vanishing contribution to the q_T soft function. Consequently, the non-zero out-cone contribution arises exclusively from the ultra-collinear-soft radiation localized near the jet boundary. For the momentum k of such a mode, we have

$$k^- \gg k^+, k_\perp, \quad (3.24)$$

where we have adopted the light-cone coordinates along the jet axis defined in eq. (3.1). Under this hierarchy, the Fourier exponent associated with the out-of-cone measurement admits the power expansion

$$\underbrace{\vec{b}_T \cdot \vec{k}_T}_{\text{beam coordinates}} = -b \cdot k \approx \underbrace{-\frac{1}{2} b^+ k^-}_{\text{jet coordinates}}, \quad (3.25)$$

with $b^\mu = (0, b_x, b_y, 0)$ and $b^+ = -b_x n_{i,x}$.

Applying the factorization framework for non-global observables [35, 36, 85] (see also [33, 34]), S_i can be expressed as

$$S_i(\vec{b}_T, \eta_i, R, \mu, \nu) = \sum_{m_i=0}^{\infty} \prod_{j=1}^{m_i} \int \frac{d\Omega(\vec{u}_j)}{4\pi} \frac{1}{d_i} \text{Tr} [\mathcal{S}_{m_i}^{\text{cs}}(\{n_i, \bar{n}_i, \underline{u}\}, b_y, R, \mu, \nu) \mathcal{S}_{m_i}^{\text{ucs}}(\{n_i, \bar{n}_i, \underline{u}\}, b_x, R, \mu)]. \quad (3.26)$$

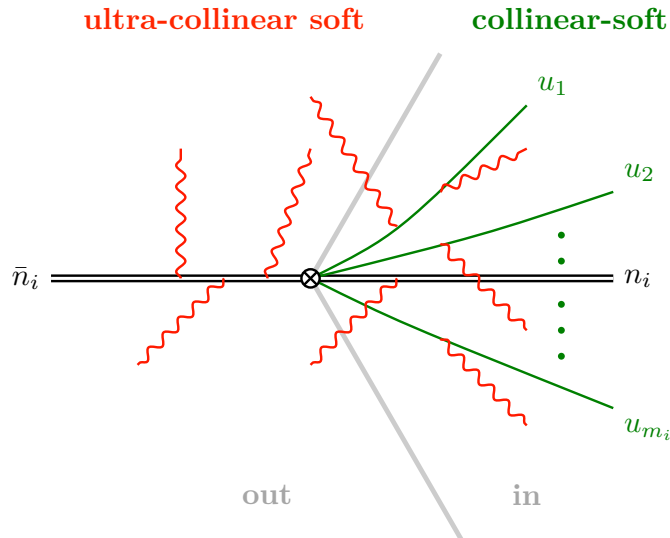


Figure 3: Pictorial representation of the factorization formula for the function S_i . The green lines correspond to the collinear-soft radiation, and the red lines represent ultra-collinear-soft emissions. Although the ultra-collinear-soft radiation contributes to the measurement only when it falls outside the jet cone, the radiation itself is not geometrically constrained and can also occur inside the jet.

Here, both the collinear-soft and ultra-collinear-soft functions are operators in color space, as indicated by the boldface notation, and therefore necessitate a color trace $\text{Tr}[\dots]$. The normalization factor d_i is N_c for quark jets and $N_c^2 - 1$ for gluon jets. They are also (diagonal) operators in the space of collinear parton multiplicities. The collinear-soft function, $\mathcal{S}_{m_i}^{\text{cs}}$, represents the squared amplitude for m_i -parton emissions from the Wilson lines along n_i and \bar{n}_i into the jet region. It is integrated over emission energies while holding the directions $\{\underline{u}\} \equiv \{u_1, \dots, u_{m_i}\}$ fixed, where $u_j^\mu = (1, \vec{u}_j)$ are light-like vectors. $\Omega(\vec{u}_j)$ denotes the solid angle of the three-vector \vec{u}_j . The ultra-collinear-soft function, $\mathcal{S}_{m_i}^{\text{ucs}}$, consists of $m_i + 2$ Wilson lines along the directions $\{\underline{u}\}$ of the m_i collinear-soft partons, the jet direction n_i , and the auxiliary light-like vector \bar{n}_i . The pictorial representation of the factorization is given in figure 3.

For notational simplicity, we use $\langle \dots \rangle$ to denote the normalized color trace $\frac{1}{d_i} \text{Tr}[\dots]$. Furthermore, we introduce the symbol \otimes to represent integration over the m_i directions of the collinear-soft emissions $\{\underline{u}\}$, which allows for a compact rewriting of S_i :

$$S_i(\vec{b}_T, \eta_i, R, \mu, \nu) = \sum_{m_i=0}^{\infty} \langle \mathcal{S}_{m_i}^{\text{ucs}}(\{n_i, \bar{n}_i, \underline{u}\}, b_x, R, \mu) \otimes \mathcal{S}_{m_i}^{\text{cs}}(\{n_i, \bar{n}_i, \underline{u}\}, b_y, R, \mu, \nu) \rangle. \quad (3.27)$$

3.3.1 Collinear-soft and ultra-collinear soft functions

We follow the notation of ref. [85] to study the multi-Wilson-line factorization framework for the collinear-soft and ultra-collinear-soft functions in the small- R limit.

The amplitudes for the emission of m_i collinear-soft partons with momenta $\{\underline{p}\}$ from the back-to-back Wilson lines along n_i and \bar{n}_i are expressed as

$$|\mathcal{M}_{m_i}^{cs}(n_i, \bar{n}_i, \{\underline{p}\})\rangle = \langle \{\underline{p}\} | S(n_i) S^\dagger(\bar{n}_i) | 0 \rangle, \quad (3.28)$$

where $|\{\underline{p}\}\rangle = \prod_{k=1}^{m_i} |p_k\rangle$ denotes the Hilbert space state of m_i partons, with momenta $p_k = E_k u_k$ and energies E_k , and $S(n_i)$ represents the collinear-soft Wilson line associated with jet i . The amplitude $|\mathcal{M}_{m_i}^{cs}(n_i, \bar{n}_i, \{\underline{p}\})\rangle$ is a vector in color space [79, 86]; hence, we employ the bra-ket notation to make this structure explicit.

In the small- R limit, since the virtuality of the collinear-soft mode is much larger than that of the ultra-collinear-soft mode, one can separate the two submodes and dress the collinear-soft field with the ultra-collinear-soft Wilson line $U_i(n_i)$,

$$U_i(n_i) = \mathbf{P} \exp \left(ig_s \int_0^\infty dt n_i \cdot A_{ucs}^a(tn_i) \mathbf{T}_i^a \right), \quad (3.29)$$

where \mathbf{T}_i encodes the color-representation information of parton i . The symbol \mathbf{P} indicates path ordering of the color matrices, ensuring that the matrix-valued field $A_{ucs}^a(tn_i)$ with the larger value of t appears to the left of those with smaller t . At the amplitude level, the ultra-collinear-soft radiation emitted from the two original Wilson lines together with the additional collinear-soft partons is described by the Wilson-line operator

$$U_a(n_i) U_b(\bar{n}_i) U_1(u_1) \cdots U_{m_i}(u_{m_i}) |\mathcal{M}_{m_i}^{cs}(n_i, \bar{n}_i, \{\underline{p}\})\rangle. \quad (3.30)$$

Now we can define the collinear-soft function in \vec{b}_T space as

$$\mathcal{S}_{m_i}^{cs}(\{n_i, \bar{n}_i, \underline{u}\}, b_y, R, \mu, \nu) = \quad (3.31)$$

$$\prod_{j=1}^{m_i} \int \frac{dE_j E_j^{d-3}}{(2\pi)^{d-2}} |\mathcal{M}_{m_i}^{cs}(n_i, \bar{n}_i, \{\underline{p}\})\rangle \langle \mathcal{M}_{m_i}^{cs}(n_i, \bar{n}_i, \{\underline{p}\}) | \exp \left(ib_y \sum_{k=1}^{m_i} p_{k,y} \right) \Theta_{\text{in}}^i(\{\underline{p}\}),$$

Here, the phase-space constraint $\Theta_{\text{in}}^i(\{\underline{p}\})$ restricts all m_i collinear-soft partons emitted from the original Wilson lines to lie inside the jet cone labeled with i . As the refactorization is carried out in the small- R limit, the in-cone constraint simplifies to

$$\Theta_{\text{in}}^i(\{\underline{p}\}) = \prod_{j=1}^{m_i} \Theta \left(R_i^2 - \frac{n_i \cdot p_j}{\bar{n}_i \cdot p_j} \right), \quad R_i = \frac{R}{2 \cosh \eta_i}. \quad (3.32)$$

The ultra-collinear-soft function in momentum space can be written as

$$\mathcal{S}_{m_i}^{\text{ucs}}(\{n_i, \bar{n}_i, \underline{u}\}, b_x, R, \mu) = \sum_{X_{ucs}} \langle 0 | U_{m_i}^\dagger(u_{m_i}) \cdots U_1^\dagger(u_1) U_b^\dagger(\bar{n}_i) U_a^\dagger(n_i) | X_{ucs} \rangle \quad (3.33)$$

$$\langle X_{ucs} | U_a(n_i) U_b(\bar{n}_i) U_1(u_1) \cdots U_{m_i}(u_{m_i}) | 0 \rangle \exp \left(-\frac{i}{2} b^+ \sum_{j \notin \text{jet}-i} k_j^- \right).$$

where $|X_{ucs}\rangle = \prod_j |k_j\rangle$, and the measurement function in the Fourier exponent captures only the unresolved ultra-collinear-soft partons outside the jet cone.

Details regarding the renormalization and anomalous dimensions of the collinear-soft and ultra-collinear-soft functions in multiplicity space are provided in appendix B.1.

4 Resummation

4.1 Azimuthal decorrelation

To resum all the large logarithms, we evolve the hard function from its natural scale μ_h to the factorization scale μ_f , which we choose equal to the natural scale for the soft and collinear sectors. We also evolve the rapidity scales of jet functions and beam functions from their respective characteristic rapidity scales $\nu_i = \omega_i$ to the soft function's rapidity scale $\nu_s = b_0/|b_y|$ with $b_0 = 2e^{-\gamma_E}$. This allows us to derive the resummation formula

$$\begin{aligned}
\frac{d^4\sigma}{d\eta_1 d\eta_2 dp_T dq_y} &= \sum_{ijkl} \frac{x_a x_b}{16\pi\hat{s}^2} \frac{2p_T}{1 + \delta_{kl}} \int_0^\infty \frac{db_y}{\pi} \cos(b_y q_y) \prod_{i=a,b,1,2} \left(\frac{\nu_s}{\nu_i}\right)^{\Gamma_\nu^i(b_y, \mu_f)} \\
&\times \sum_{KK'} \exp \left\{ \int_{\mu_h}^{\mu_f} \frac{d\mu}{\mu} \left[\gamma_{\text{cusp}}(\alpha_s) \left(C_H \ln \frac{\hat{s}}{\mu^2} + \lambda_K + \lambda_{K'}^* \right) + 2\gamma_H(\alpha_s) \right] \right\} \\
&\times \mathcal{H}_{ij \rightarrow k\ell, KK'}(p_T, \eta_1 - \eta_2, \mu_h) \mathcal{S}_{ijk\ell, K'K}(b_y, \eta_1, \eta_2, \mu_f, \nu_s) \\
&\times B_{i/p}(x_a, \omega_a, b_y, \mu_f, \nu_a) B_{j/p}(x_b, \omega_b, b_y, \mu_f, \nu_b) \\
&\times \mathcal{J}_k(b_y, \omega_1, \mu_f, \nu_1) \mathcal{J}_\ell(b_y, \omega_2, \mu_f, \nu_2) \\
&\times \exp \left[-S_{\text{NP}}^i(b_y, Q_0, \omega_a) - S_{\text{NP}}^j(b_y, Q_0, \omega_b) \right], \tag{4.1}
\end{aligned}$$

where λ_K are the eigenvalues of $\mathbf{M}_{ij \rightarrow k\ell}$ in the hard function's anomalous dimensions. Here, $\mu_h = v_h 2p_T$ and $\mu_f = \min\{v_f \mu_{b_{y,*}}, \mu_h\}$, where v_h and v_f are scale-variation parameters used to estimate theoretical uncertainties. Our central curves in section 5 are obtained with $v_h = v_f = 1$, and uncertainty bands correspond to varying $v_h, v_f \in [0.5, 2]$.

To avoid the Landau pole at large b_y , we adopt the b_* prescription,

$$b_{y,*} = \frac{|b_y|}{\sqrt{1 + b_y^2/b_{\text{max}}^2}}, \quad \mu_{b_{y,*}} = \frac{b_0}{b_{y,*}}, \tag{4.2}$$

with $b_{\text{max}} = 1.5 \text{ GeV}^{-1}$. To account for non-perturbative effects that dominate at large impact parameters b , we introduce a non-perturbative Sudakov form factor, S_{NP} [87–91]. Specifically, its explicit form is given by

$$S_{\text{NP}}^i(b, Q_0, Q) = g_1 b^2 + \frac{g_2 C_i}{2 C_F} \ln \frac{Q}{Q_0} \ln \frac{b}{b_*}, \tag{4.3}$$

where the first term parametrizes the Gaussian shape and the second term captures the non-perturbative evolution. Here, C_i is the quadratic Casimir. For the numerical evaluation, we employ the fitting parameters at $Q_0^2 = 2.4 \text{ GeV}^2$ obtained from ref. [91]: $g_1 = 0.106 \text{ GeV}^2$, $g_2 = 0.84$.

4.2 Transverse momentum imbalance

In the subsequent resummation, performed in the conjugate \vec{b}_T -space, the soft (global soft function) and initial collinear (beam function) modes are assigned a common scale $\mu_s \sim \mu_b$,

while the collinear-soft and final collinear (jet function) modes share the scale $\mu_{cs} \sim \mu_j$. The ultra-collinear-soft mode is characterized by its own scale μ_{ucs} . Their typical values are

$$\mu_b \sim \mu_s \sim b_0/b_T, \quad \mu_{cs} \sim \mu_j \sim b_0/|b_y|, \quad \mu_{ucs} \sim R b_0/(2|b_x|), \quad (4.4)$$

together with the hard scale $\mu_h \sim 2p_T$. We again choose the factorization scale as the common scale of the beam and the global-soft functions, $\mu_f \sim b_0/b_T$. Since the two groups of modes share common virtualities within each group, we employ the RRG framework to handle the associated rapidity divergences [68, 69]. The characteristic rapidity scales for different modes are given by

$$\nu_i \sim \omega_i \ (i = a, b, 1, 2), \quad \nu_s \sim b_0/b_T, \quad \nu_{cs,i} \sim b_0/(|b_y|R_i) \ (i = 1, 2). \quad (4.5)$$

It is also worth noting that though the virtualities of the soft and collinear-soft modes are parametrically of the same order, their numerical values are not identical. Therefore, the renormalization group (RG) evolution from μ_{cs} to μ_f should be included to resum the large logarithms $\ln(|b_y|/b_T)$ that arise in the limit $\sin \phi_b \rightarrow 0$.

After analyzing the modes and scales, we proceed with the RRG and RG evolution. The rapidity scales of the beam functions are evolved from $\nu_i = x_i\sqrt{s}$ ($i = a, b$) to the rapidity scale of the global soft function, $\nu_s = b_0/b_T$. Similarly, the rapidity scales of the jet functions should first be evolved from $\nu_i = 2p_T \cosh \eta_i$ ($i = 1, 2$) to the rapidity scale of the collinear-soft function, $\nu_{cs,i} = b_0/(|b_y|R_i)$. The rapidity scale evolution takes the form of

$$\prod_{i=ab} \left(\frac{\nu_s}{\nu_i} \right)^{\Gamma_{\nu}^i(b_T, \mu_f)} \prod_{i=12} \left(\frac{\nu_{cs,i}}{\nu_i} \right)^{\Gamma_{\nu}^i(b_y, \mu_{cs})} = \prod_{i=ab} \left(\frac{b_0}{b_T x_i \sqrt{s}} \right)^{\Gamma_{\nu}^i(b_T, \mu_f)} \prod_{i=12} \left(\frac{b_0}{|b_y| p_T R} \right)^{\Gamma_{\nu}^i(b_y, \mu_{cs})}. \quad (4.6)$$

Next, we consider the RG evolution to the factorization scale. The RG evolution of the hard function is analogous to that for the q_y distribution, while the jet, collinear-soft, and ultra-collinear-soft functions require additional clarification. The evolution matrix for these functions can be schematically written as

$$\begin{aligned} U &= \exp \left[\int_{\mu_j}^{\mu_f} \frac{d\mu}{\mu} \Gamma^{J_i} \right] \mathbf{P} \exp \left[\int_{\mu_{cs}}^{\mu_f} \frac{d\mu}{\mu} \Gamma^{\text{cs}} - \int_{\mu_{ucs}}^{\mu_f} \frac{d\mu}{\mu} \Gamma^{\text{ucs}} \right] \\ &= \exp \left[\int_{\mu_{cs}}^{\mu_f} \frac{d\mu}{\mu} (\Gamma^{J_i} + \Gamma^{\text{cs}} + \Gamma^{\text{ucs}}) \right] \mathbf{P} \exp \left[- \int_{\mu_{ucs}}^{\mu_{cs}} \frac{d\mu}{\mu} \Gamma^{\text{ucs}} \right], \end{aligned} \quad (4.7)$$

where the jet scale μ_j is the same as the collinear-soft scale μ_{cs} . The separation of the anomalous dimensions for $\Gamma^{\text{cs, ucs}}$ in multiplicity space is defined in eqs. (B.31) and (B.32), while the explicit expressions for their global parts, $\Gamma^{\text{cs, ucs}}$, are given in eqs. (B.34) and (B.35).

After combining the evolution matrices for the collinear-soft and ultra-collinear-soft functions from μ_{cs} to the factorization scale μ_f , the multiplicity mixing arises only in the

second exponential term of the following evolution

$$\exp \left[- \int_{\mu_{ucs}}^{\mu_{cs}} \frac{d\mu}{\mu} \mathbf{\Gamma}^{\text{ucs}} \right] = \exp \left[\int_{\mu_{ucs}}^{\mu_{cs}} \frac{d\mu}{\mu} \mathbf{\Gamma}^{\text{ucs}} \right] \mathbf{P} \exp \left[- \int_{\mu_{ucs}}^{\mu_{cs}} \frac{d\mu}{\mu} \hat{\mathbf{\Gamma}} \right]. \quad (4.8)$$

We can define the multiplicity-mixing evolution matrix in a more rigorous manner. To resum the leading NGLs in R (denoted as LL $_R$), one can retain only the tree-level contribution of the ultra-collinear-soft function, $\mathbf{S}_m^{\text{ucs}} = \mathbf{1} + \mathcal{O}(\alpha_s)$, together with the leading-order collinear-soft function, $\mathbf{S}_0^{\text{cs}} = \mathbf{1}$, to evaluate

$$U_{\text{NG}}^i(\mu_{ucs}, \mu_{cs}) \stackrel{\text{LL}_R}{=} \sum_{m=0}^{\infty} \langle \mathbf{1} \hat{\otimes} \mathbf{U}_{m0}(\{n_i, \bar{n}_i, \underline{u}\}, \mu_{ucs}, \mu_{cs}) \rangle, \quad (4.9)$$

where $\mathbf{U}(\{n_i, \bar{n}_i, \underline{u}\}, \mu_{ucs}, \mu_{cs}) \equiv \mathbf{P} \exp \left[- \int_{\mu_{ucs}}^{\mu_{cs}} d \ln \mu \hat{\mathbf{\Gamma}}(\{\underline{n}\}, \mu) \right]$.

As shown in the appendix C, the ultra-collinear-soft and collinear-soft functions defined here can be interpreted as hemisphere soft functions after performing a Lorentz boost along the jet axis, analogous to the constructions in [36, 92]. Following the procedure outlined in [40], the non-global evolution matrix from the ultra-collinear-soft scale to the collinear-soft scale can be approximated using the Dasgupta–Salam parametrization [31],

$$U_{\text{NG}}^i(\mu_{ucs}, \mu_{cs}) \approx \exp \left(-C_A C_i \frac{\pi^2}{3} u^2 \frac{1 + (au)^2}{1 + (bu)^c} \right), \quad u = \frac{1}{\beta_0} \ln \frac{\alpha_s(\mu_{ucs})}{\alpha_s(\mu_{cs})}, \quad (4.10)$$

with the constants given by $a = 0.85C_A$, $b = 0.86C_A$ and $c = 1.33$. One can resum the leading NGL contributions using eq. (4.10) in the subsequent NLL and NNLL resummations.

Therefore, the combined RG evolution for the jet, collinear-soft and ultra-collinear-soft functions is given by

$$\prod_{i=1,2} \exp \left[\int_{\mu_{cs}}^{\mu_f} \frac{d\mu}{\mu} (\Gamma^{J_i} + \Gamma_i^{\text{cs}}) + \int_{\mu_{ucs}}^{\mu_f} \frac{d\mu}{\mu} \Gamma_i^{\text{ucs}} \right] U_{\text{NG}}^i(\mu_{ucs}, \mu_{cs}). \quad (4.11)$$

After evolving the rapidity scales of the jet functions, ν_i ($i = 1, 2$), to the rapidity scale of the corresponding collinear-soft functions $\nu_{cs,i}$ ($i = 1, 2$), we can combine the jet and collinear-soft contributions and perform their RG evolution together, yielding

$$\begin{aligned} U^{\text{jet+cs}}(\mu_{cs}, \mu_f) &= \prod_{i=1,2} \exp \left[\int_{\mu_{cs}}^{\mu_f} \frac{d\mu}{\mu} (\Gamma^{J_i} + \Gamma_i^{\text{cs}}) \right] \\ &= \prod_{i=1,2} \exp \left\{ \int_{\mu_{cs}}^{\mu_f} \frac{d\mu}{\mu} \sum_{i=1}^2 \left[C_i \gamma_{\text{cusp}} \ln \frac{\mu^2}{p_T^2 R^2} + \gamma_{nc,i} \right] \right\} \\ &= \prod_{i=1}^2 \left[\exp \left(-2C_i S(\mu_{cs}, \mu_f) - A_{\gamma_{nc,i}}(\mu_{cs}, \mu_f) \right) \left(\frac{p_T^2 R^2}{\mu_{cs}^2} \right)^{C_i A \gamma_{\text{cusp}}(\mu_{cs}, \mu_f)} \right], \end{aligned} \quad (4.12)$$

where the cusp γ_{cusp} and the non-cusp anomalous dimension $\gamma_{nc,i} = \gamma^{J_i} + \mathcal{O}(\alpha_s^3)$ are given in appendix D. The perturbative expression of $S(\nu, \mu)$ and $A_\gamma(\nu, \mu)$ are shown in the appendix

of [93]. As for the global evolution of the ultra-collinear-soft function, it takes the form

$$\begin{aligned}
U^{ucs}(\mu_{ucs}, \mu_f) &= \prod_{i=1,2} \exp \left[\int_{\mu_{ucs}}^{\mu_f} \frac{d\mu}{\mu} \Gamma_i^{ucs} \right] \\
&= \prod_{i=1,2} \exp \left[2C_i S(\mu_{ucs}, \mu_f) - i\pi C_i A_{\gamma_{\text{cusp}}}(\mu_{ucs}, \mu_f) \text{Sign}(\cos(\phi_b - \phi_i)) \right] \\
&\quad \times \prod_{i=1,2} \left(\frac{R^2 b_0^2 / (4b_T^2 \cos^2 \phi_b)}{\mu_{ucs}^2} \right)^{-C_i A_{\gamma_{\text{cusp}}}(\mu_{ucs}, \mu_f)}, \tag{4.13}
\end{aligned}$$

which also contributes to the resummation of logarithms of the jet radius.

To prepare for the NNLL resummation, we now present the renormalized collinear-soft and ultra-collinear-soft functions at NLO accuracy. Their corresponding bare expressions are given in appendix B. After integrating out the angular dependence, the NLO collinear-soft function contributes to S_i as

$$\begin{aligned}
&\langle \mathbf{1} \otimes \mathbf{S}_1^{\text{cs}}(\{n_i, \bar{n}_i, u_1\}, b_y, R, \mu, \nu) \rangle \\
&= \frac{\alpha_s(\mu)}{4\pi} C_i \left[-\ln^2 \frac{\mu^2 b_y^2}{b_0^2} + 4 \ln \frac{\mu^2 b_y^2}{b_0^2} \left(\ln \frac{\mu}{\nu} + \ln \frac{2 \cosh \eta_i}{R} \right) - \frac{\pi^2}{6} \right] + \mathcal{O}(\alpha_s^2), \tag{4.14}
\end{aligned}$$

where $\mathbf{S}_1^{\text{ucs}} = \mathbf{1} + \mathcal{O}(\alpha_s)$. Only the tree-level term of $\mathbf{S}_1^{\text{ucs}}$ is required for the NLO expansion of S_i as shown in eq. (4.14), because $\mathbf{S}_{m_i}^{\text{cs}} \sim \mathcal{O}(\alpha_s^{m_i})$. Meanwhile, the ultra-collinear-soft function contributing to S_i up to NLO accuracy takes the form

$$\begin{aligned}
\langle \mathbf{S}_0^{\text{ucs}}(\{n_i, \bar{n}_i\}, \vec{b}_T, R, \mu) \rangle &= 1 + \frac{\alpha_s(\mu)}{4\pi} C_i \left[-4 \ln^2 \left(\frac{-2i \cos(\phi_b - \phi_i) \mu b_T}{b_0 R} \right) - \frac{\pi^2}{2} \right] + \mathcal{O}(\alpha_s^2) \\
&= 1 + \frac{\alpha_s(\mu)}{4\pi} C_i \left\{ -4 \left[\ln \left(\frac{\mu}{b_0 R / (2|b_x|)} \right) - i \frac{\pi}{2} \text{Sign}(n_{i,x} b_x) \right]^2 - \frac{\pi^2}{2} \right\} + \mathcal{O}(\alpha_s^2). \tag{4.15}
\end{aligned}$$

Given that we have $\mathbf{S}_0^{\text{cs}} = \mathbf{1}$, and no additional collinear parton directions need to be integrated over, we omit the term $\otimes \mathbf{S}_0^{\text{cs}}$ inside the color trace.

In conclusion, the NNLL resummation formula is given by

$$\begin{aligned}
&\frac{d^5 \sigma}{d\eta_1 d\eta_2 dp_T dq_T d\phi_q} \\
&= \sum_{ijkl} \frac{x_a x_b}{16\pi \hat{s}^2} \frac{2p_T}{1 + \delta_{k\ell}} q_T \int_0^{2\pi} d\phi_b \int_0^\infty \frac{b_T db_T}{(2\pi)^2} e^{i\vec{q}_T \cdot \vec{b}_T} \\
&\quad \times \sum_{KK'} \exp \left\{ \int_{\mu_h}^{\mu_f} \frac{d\mu}{\mu} \left[\gamma_{\text{cusp}}(\alpha_s) \left(C_H \ln \frac{\hat{s}}{\mu^2} + \lambda_K + \lambda_{K'}^* \right) + 2\gamma_H(\alpha_s) \right] \right\} \\
&\quad \times \prod_{p=ab} \left(\frac{\nu_s}{\nu_p} \right)^{\Gamma_p^{\nu}(b_T, \mu_f)} \prod_{p=12} \left(\frac{\nu_{\text{cs},p}}{\nu_p} \right)^{\Gamma_p^{\nu}(b_y, \mu_{\text{cs}})}
\end{aligned}$$

$$\begin{aligned}
& \times \prod_{p=12} \exp \left[\int_{\mu_{cs}}^{\mu_f} \frac{d\mu}{\mu} (\Gamma^{J_p} + \Gamma_p^{cs}) + \int_{\mu_{ucs}}^{\mu_f} \frac{d\mu}{\mu} \Gamma_p^{ucs} \right] U_{\text{NG}}^p(\mu_{ucs}, \mu_{cs}) \\
& \times \mathcal{H}_{ij \rightarrow k\ell, KK'}(p_T, \eta_1 - \eta_2, \mu_h) \mathcal{S}_{ijkl, K'K}^{\text{global}}(\vec{b}_T, \eta_1, \eta_2, \mu_f, \nu_s) \\
& \times \prod_{p=12} \sum_{m_p=0}^{\infty} \left\langle \mathcal{S}_{m_p}^{ucs}(\{n_p, \bar{n}_p, \underline{u}\}, \vec{b}_T, R, \mu_{ucs}) \otimes \mathcal{S}_{m_p}^{cs}(\{n_p, \bar{n}_p, \underline{u}\}, b_y, R, \mu_{cs}, \nu_{cs,p}) \right\rangle \\
& \times B_{i/p}(x_a, b_T, \omega_a, \mu_f, \nu_a) B_{j/p}(x_b, b_T, \omega_b, \mu_f, \nu_b) \mathcal{J}_k(b_y, \omega_1, \mu_j, \nu_1) \mathcal{J}_\ell(b_y, \omega_2, \mu_j, \nu_2) \\
& \times \exp \left[-S_{\text{NP}}^i(b_T, \omega_a, \nu_a) - S_{\text{NP}}^j(b_T, \omega_b, \nu_b) \right]. \tag{4.16}
\end{aligned}$$

To avoid the Landau poles in the resummation formula, we adopt the b_* -prescription,

$$b_{T,*} = \frac{b_T}{\sqrt{1 + b_T^2/b_{\text{max}}^2}}, \quad b_{y,*} = \frac{|b_y|}{\sqrt{1 + b_y^2/b_{\text{max}}^2}}, \quad b_{x,*} = \frac{|b_x|}{\sqrt{1 + b_x^2/b_{\text{max}}^2}}. \tag{4.17}$$

With the exception of the hard scale $\mu_h = v_h 2p_T$, all other perturbative scales are obtained through this prescription as

$$\mu_s = \mu_b = \mu_f = \min \left\{ v_f \frac{b_0}{b_{T,*}}, \mu_h \right\}, \quad \mu_j = \mu_{cs} = v_f \frac{b_0}{b_{y,*}}, \quad \mu_{ucs} = \min \left\{ v_f \frac{Rb_0}{2b_{x,*}}, \mu_{cs} \right\}. \tag{4.18}$$

With v_h and v_f varied in the range $[0.5, 2]$, we evaluate the theoretical uncertainty associated with the hard scale, as well as the uncertainties from μ_f , μ_{cs} , and μ_{ucs} , by varying them simultaneously, as discussed in section 5. To respect the RG flow from the ultraviolet to the infrared, we require the factorization scale μ_f to be bounded by the hard scale μ_h , $\mu_f \leq \mu_h$. Furthermore, to preserve the scale hierarchy inherent to the small- R refactorization and ensure the positivity of the evolution variable u in eq. (4.10), we impose the constraint $\mu_{ucs} \leq \mu_{cs}$.

5 Numerical results

In this section, we present our numerical predictions for the azimuthal decorrelation $\delta\phi$ and the transverse momentum imbalance q_T in inclusive dijet production at the LHC. We perform the calculation at a center-of-mass energy of $\sqrt{s} = 13$ TeV. Jets are identified using the anti- k_T clustering algorithm [94] with a radius parameter $R = 0.5$ and the standard E -scheme [62] for recombination. The kinematic acceptance is defined by the following cuts on the standard E -scheme transverse momenta of the leading ($p_{T,1}$) and subleading ($p_{T,2}$) jets, as well as their rapidities,

$$p_{T,1} > 100 \text{ GeV}, \quad p_{T,2} > 80 \text{ GeV}, \quad |\eta_{1,2}| < 2.0. \tag{5.1}$$

As detailed in the previous sections, the observables $\delta\phi$ and q_T are defined with respect to the reconstructed winner-take-all (WTA) axis³, which minimizes sensitivity to NGLs.

³To avoid losing particles due to the mismatch between the WTA axis and the original axis, we recluster in the WTA scheme with a larger jet radius.

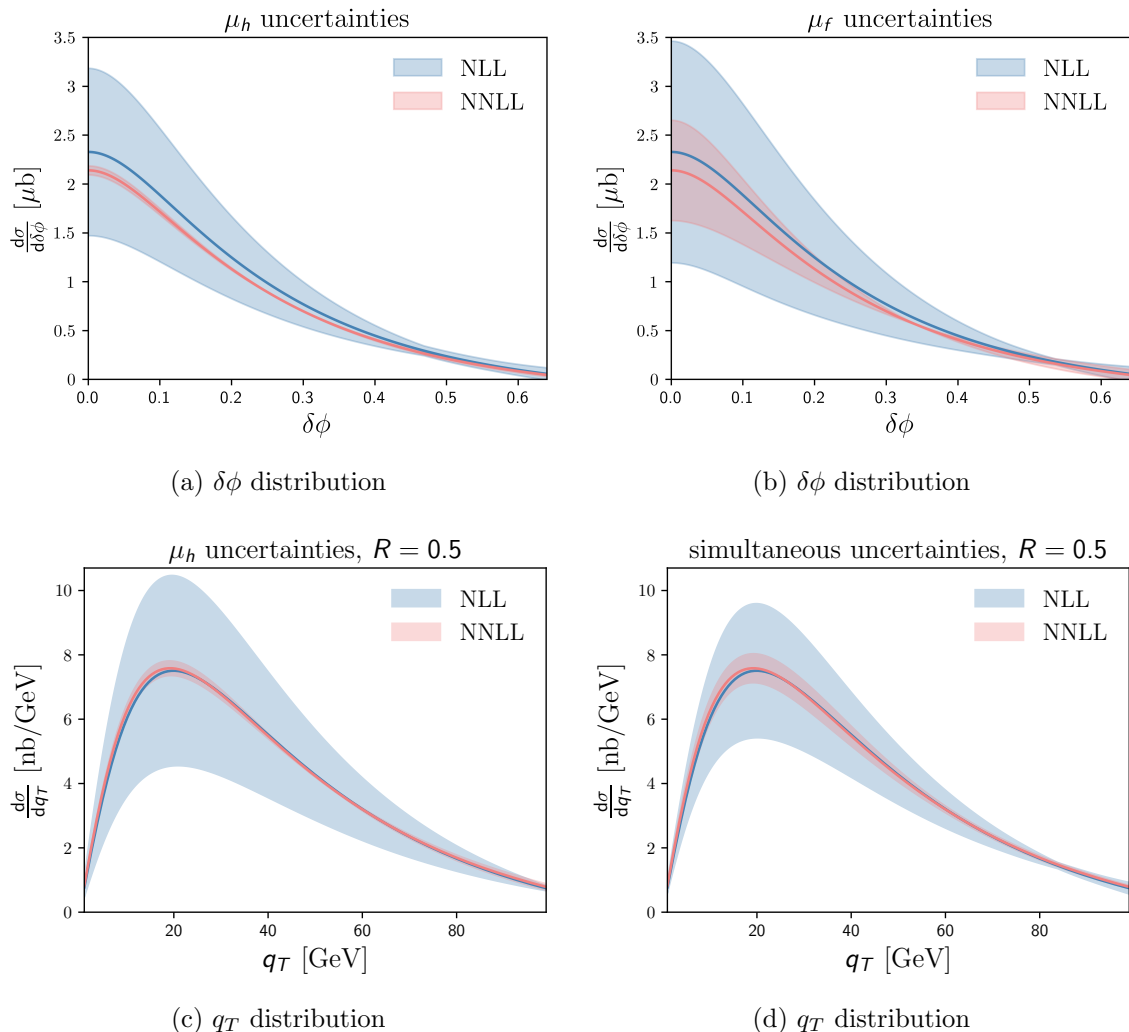


Figure 4: Theoretical uncertainties for the resummed $\delta\phi$ (top row) and q_T (bottom row, $R = 0.5$) distributions. The blue and red bands represent NLL and NNLL predictions, respectively. The left column (a, c) shows the uncertainty derived from varying the hard scale μ_h by factors of 2 and 0.5 around its central value $2p_T$. The right column (b, d) displays the scale uncertainties from the factorization scale μ_f (for $\delta\phi$) and the simultaneous variation of factorization, collinear-soft and ultra-collinear-soft scales (for q_T).

For the fixed-order components required for the NLO matching procedure, we utilize NLOJET++ and FASTJET to compute the LO differential cross sections for the 3-parton production process. We also compare our matched predictions with parton-shower results obtained from PYTHIA 8 to assess the impact of non-perturbative effects.

5.1 NNLL resummation

In figure 4, we present the resummed differential cross sections for the azimuthal decorrelation $\delta\phi$ (top row) and the transverse momentum imbalance q_T (bottom row). The blue

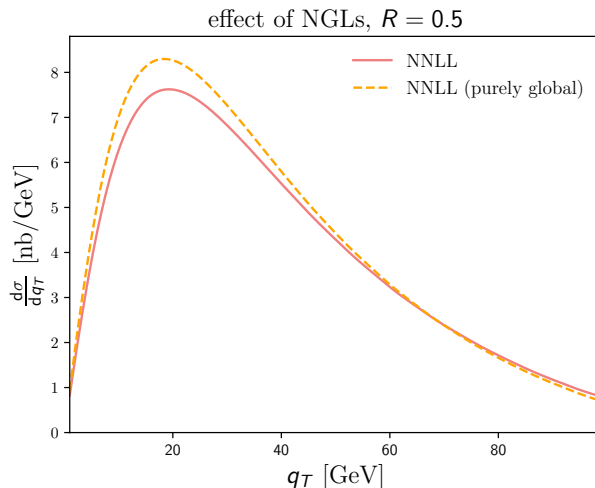


Figure 5: The impact of the resummation of NGLs on the q_T distribution for a jet radius of $R = 0.5$. The solid red curve represents the full NNLL result including the non-global resummation factor U_{NG} , while the dashed orange curve shows the “purely global” NNLL prediction where the contribution from U_{NG} is turned off.

bands correspond to NLL accuracy, while the red bands denote the NNLL results. We observe a substantial reduction in theoretical scale uncertainties for both observables when advancing from NLL to NNLL accuracy.

For the $\delta\phi$ distribution, as shown in figure 4(a), the uncertainty associated with the hard scale μ_h becomes almost negligible at NNLL. The factorization scale uncertainty (figure 4(b)) also decreases markedly, though it remains the dominant source of theoretical uncertainty. Crucially, the NNLL bands lie consistently within the NLL envelopes, demonstrating the excellent perturbative convergence of our factorization framework.

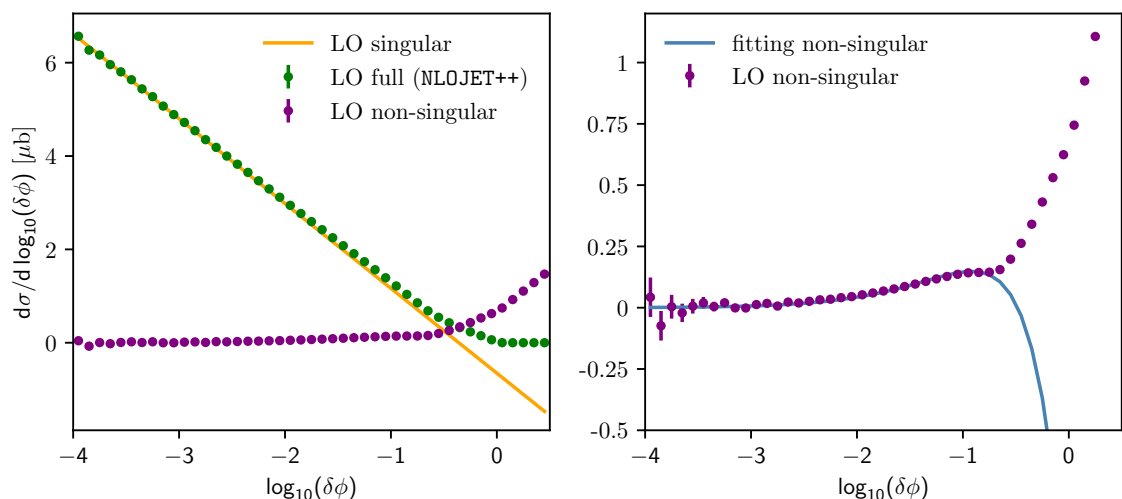
Similar behavior is observed for the q_T distribution, calculated with $R = 0.5$. Figure 4(c) shows a drastic reduction in hard scale dependence at NNLL. Figure 4(d) presents the uncertainty arising from the simultaneous variation of the factorization scale μ_f and the associated soft scales (μ_{cs} and μ_{ucs}). While this remains the dominant uncertainty, the bandwidth is substantially reduced. The distribution peaks in the perturbative region around $q_T \sim 18\text{--}22$ GeV, and the overlap between the NLL and NNLL orders confirms the reliability of the resummation framework.

We have also investigated the effect on the q_T distribution of the resummation of NGLs by U_{NG} , shown in figure 5.

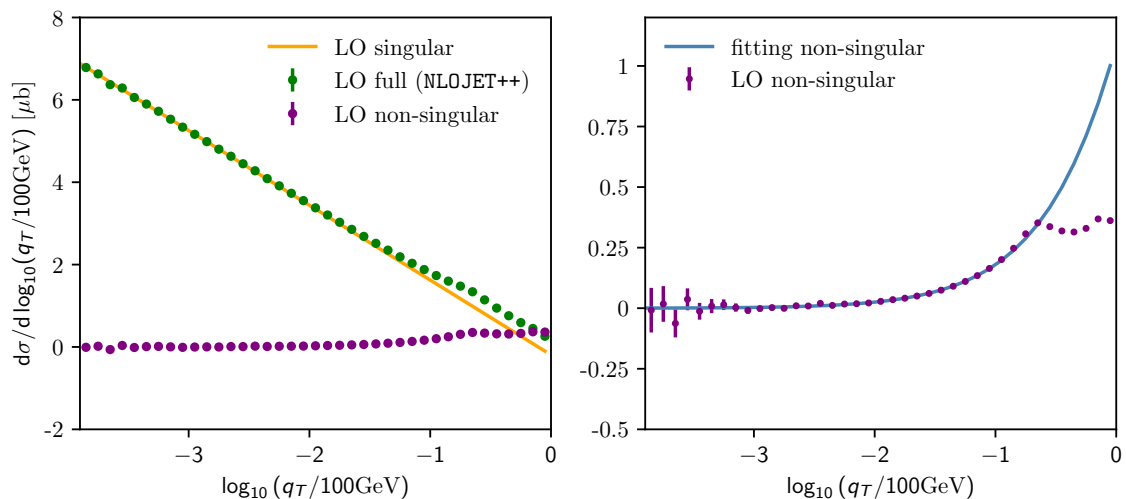
5.2 Power corrections and NLO matching

5.2.1 Power corrections

In this section, we validate the singular components of our factorization formulae against fixed-order results generated by NLOJET++ at LO, representing the Born-level 3-parton



(a) The azimuthal decorrelation $\delta\phi$.



(b) The transverse momentum imbalance q_T .

Figure 6: Validation of factorization and power corrections for the observables (a) and (b). In the left column, the full LO differential cross sections from NLOJET++ (green points) are compared with the singular contributions predicted by our factorization formulae (solid orange lines); their difference yields the non-singular terms (purple points). In the right column, the non-singular power corrections are fitted to the functional form $f(\mathcal{O}) = a\mathcal{O} + b\mathcal{O}\ln\mathcal{O}$ (blue lines). The fit is performed over the range $\log_{10}(\delta\phi) \in [-3.0, -0.7]$ for azimuthal decorrelation, and $\log_{10}(q_T/100\text{ GeV}) \in [-3.9, -1.0]$ for transverse momentum imbalance. The kinematic cuts imposed on the jets are summarized in eq. (5.1).

production. Figure 6 displays the results for the azimuthal decorrelation $\delta\phi$ (top row) and the transverse momentum imbalance q_T (bottom row).

The left panels of figure 6 demonstrate that in the deep infrared regions, specifically

$\delta\phi \ll 1$ and $q_T \ll p_T$, the predicted singular distributions (solid orange lines) converge precisely with the full LO calculations (green points). This agreement confirms the accuracy of the singular factorization formulae derived in sections 3.1 and 3.2.

In the right panels, we isolate the non-singular power corrections (purple points), defined as the difference between the full theory and the singular terms. To capture the behavior of these corrections, we fit the data (blue curves) using a logarithmic ansatz of the form $a\mathcal{O} + b\mathcal{O} \ln \mathcal{O}$, where \mathcal{O} represents either $\delta\phi$ or q_T . For instance, the $\delta\phi$ corrections are well described by this function over the range $\log_{10}(\delta\phi) \in [-3.0, -0.7]$.

To interpret the physical implications of this fit, we decompose the cross section into singular and power-correction terms. The logarithmic distribution (as plotted) and the linear differential distribution are given by

$$\begin{aligned} \frac{d\sigma(\text{LO full})}{d \log_{10} \mathcal{O}} &\simeq \frac{d\sigma(\text{LO singular})}{d \log_{10} \mathcal{O}} + \frac{d\sigma(\text{power corrections})}{d \log_{10} \mathcal{O}} \\ &= (A_1 \ln \mathcal{O} + A_0) + (B_1 \mathcal{O} + B_0 \mathcal{O} \ln \mathcal{O}), \\ \frac{d\sigma(\text{LO full})}{d\mathcal{O}} &\simeq \frac{A_1 \ln \mathcal{O} + A_0}{\mathcal{O}} + (B_1 + B_0 \ln \mathcal{O}). \end{aligned} \quad (5.2)$$

Here, the coefficients A_1 and A_0 parameterize the leading-power singular behavior, while B_1 and B_0 characterize the non-singular contributions. Notably, as shown in eq. (5.2), the non-singular contribution $(B_1 + B_0 \ln \mathcal{O})$ retains a logarithmic divergence as $\mathcal{O} \rightarrow 0$, despite being suppressed relative to the leading singular terms.

This logarithmic enhancement is characteristic of exclusive or jet-dependent observables [95–99]. This stands in contrast to the behavior of inclusive quantities, such as the Drell-Yan transverse momentum spectrum, which takes the form (see e.g., [100, 101])

$$\frac{d\sigma^{\text{LO}}}{dq_T} = \frac{A_1 \ln q_T + A_0}{q_T} + (C_1 \ln q_T + C_0)q_T + \dots, \quad (5.3)$$

where A_i and C_i are constant coefficients. In that framework, the power corrections $((C_1 \ln q_T + C_0)q_T)$ vanish as $q_T \rightarrow 0$. Conversely, the presence of the $b \ln \mathcal{O}$ term in our analysis implies that power corrections in our paper are more singular than those in inclusive Drell-Yan, diverging logarithmically rather than vanishing in the infrared limit.

5.2.2 NLO matching

The explicit expression for the *naive* additive matching prescription, used to match the NNLL resummation curve to the LO fixed-order result, is

$$d\sigma_{\text{add}}(\text{NNLL} + \text{LO}) = d\sigma(\text{NNLL}) + \underbrace{d\sigma(\text{LO full}) - d\sigma(\text{LO singular})}_{d\sigma(\text{LO non-singular})}. \quad (5.4)$$

The $d\sigma(\text{LO non-singular})$ term defined here, also known as the matching correction, is dominated by $d\sigma(\text{power corrections})$ in the small \mathcal{O} region.

However, two issues remain to be resolved in the matching procedure. First, in the small- \mathcal{O} region, divergent power corrections of the form $a + b \ln \mathcal{O}$ degrade the quality of

the matching, which is the main reason for the poor performance of the naive additive scheme in our case. Second, since factorization breaks down in the large- \mathcal{O} region and the resummed result contains Sudakov effects beyond the fixed-order accuracy, this unphysical contribution must be removed to recover the pure fixed-order prediction.

To address the first issue, we utilize an effective evolution matrix U_H^{eff} to resum the large logarithm $\ln \mathcal{O}$ in the small \mathcal{O} region of matching corrections,

$$U_H^{\text{eff}}(\mathcal{O}) = \exp \left[\int_{2p_T}^{\mu_{\mathcal{O}}} \frac{d\mu}{\mu} \left(\frac{\alpha_s(2p_T)}{\pi} 4C_A \ln \frac{4p_T^2}{\mu^2} \right) \right], \quad (5.5)$$

with $p_T = 100$ GeV. For the $\delta\phi$ distribution, we set $\mu_{\mathcal{O}} = p_T\delta\phi$, while $\mu_{\mathcal{O}} = q_T$ for the q_T distribution. Eq. (5.5) corresponds to the evolution matrix of the $gg \rightarrow gg$ channel at double-logarithmic accuracy, with the coupling constant fixed at the hard scale $2p_T$ and non-diagonal anomalous dimensions neglected. The effective Sudakov factors for q_T and $\delta\phi$ distribution are shown in figure 7.

As for the second issue, a transition function $t(\mathcal{O})$ can be introduced to smoothly switch off the resummation and transition to the fixed order:

$$t(\delta\phi) = \frac{1}{2} - \frac{1}{2} \tanh \left(4 - \frac{2\delta\phi}{r} \right), \quad t(q_T) = \begin{cases} 0, & q_T \leq 1 \text{ GeV}, \\ \frac{1}{2} - \frac{1}{2} \tanh \left(4 - \frac{2q_T}{r} \right), & q_T > 1 \text{ GeV}. \end{cases} \quad (5.6)$$

A cutoff is applied in the transition function for the q_T distribution because the LO singular term obtained from NLOJET++ becomes excessively large in the small- q_T region.

Accordingly, the modified additive matching scheme is defined as

$$\begin{aligned} d\sigma_{\text{match}}(\text{NNLL} + \text{LO}) &= (1 - t(\mathcal{O})) \left(d\sigma(\text{NNLL}) + U_H^{\text{eff}}(\mathcal{O}) d\sigma(\text{LO non-singular}) \right) \\ &+ t(\mathcal{O}) d\sigma(\text{LO full}). \end{aligned} \quad (5.7)$$

Figure 7 illustrates the behavior of the two regulating functions introduced in our modified matching scheme. The top panels depict the effective evolution matrix, $U_H^{\text{eff}}(\mathcal{O})$. As the observable \mathcal{O} approaches zero, the Sudakov suppression causes U_H^{eff} to vanish. This behavior is crucial: it effectively dampens the divergent non-singular contributions (discussed in the previous section) in the deep infrared limit, thereby stabilizing the numerical matching where the naive additive scheme would fail.

The bottom panels of figure 7 display the transition function $t(\mathcal{O})$ for different values of the profile parameter r . This function acts as a smooth switch, transitioning from 0 in the resummation-dominated region to 1 in the fixed-order region. By varying r , we shift the transition point, allowing us to estimate the uncertainty associated with the matching procedure. Concretely, for matching $\delta\phi$, we vary $r \in [0.12, 0.24]$, while for q_T , we vary $r \in [20, 30]$ GeV. This mechanism ensures that unphysical Sudakov effects are removed at large $\delta\phi$ or q_T , seamlessly recovering the correct LO cross section in the tail of the distribution.

The final matched results for the $\delta\phi$ and q_T distributions are presented in figure 8, with the top and bottom rows corresponding to $\delta\phi$ and q_T , respectively. In the left panels

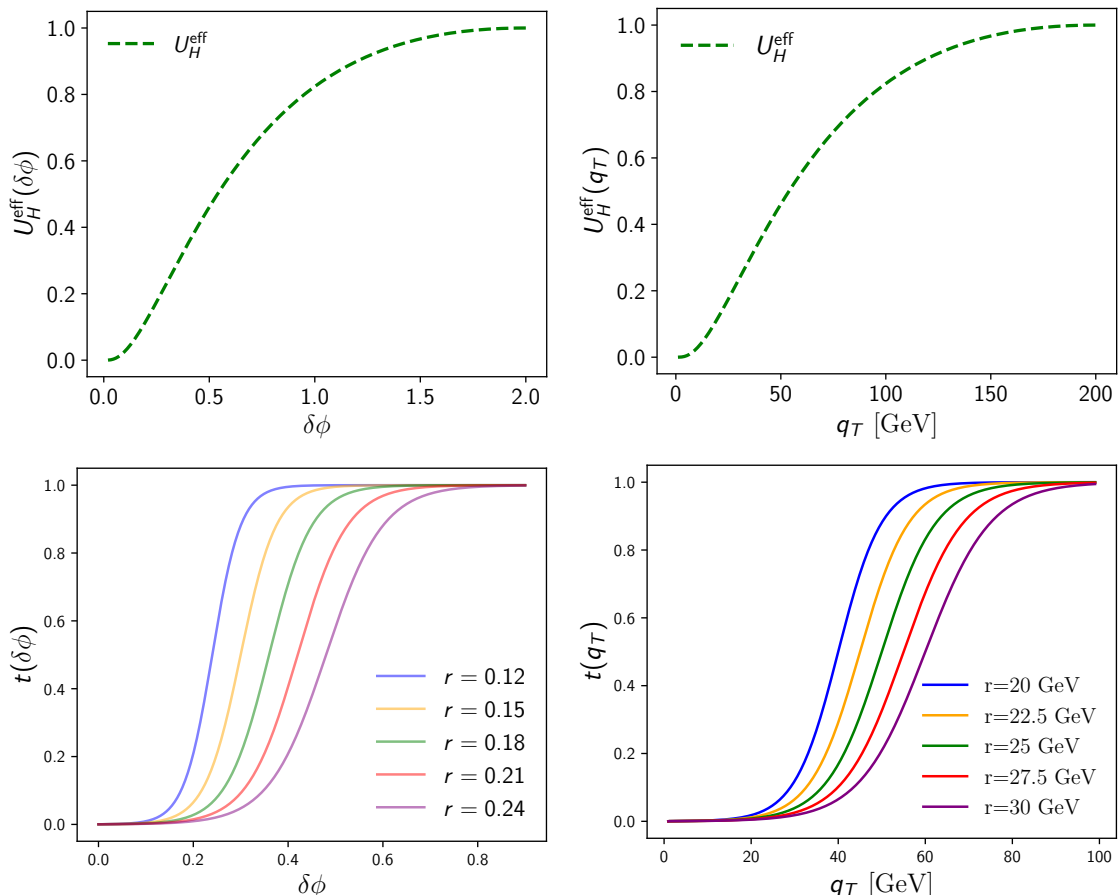


Figure 7: Key components of the modified additive matching scheme. The top row displays the effective evolution matrix $U_H^{\text{eff}}(\mathcal{O})$ for $\mathcal{O} = \delta\phi$ (left) and q_T (right). This factor is applied to the matching correction to suppress the divergence of power corrections in the deep infrared region ($\mathcal{O} \rightarrow 0$). The bottom row shows the transition profiles $t(\delta\phi)$ (left) and $t(q_T)$ (right) for various transition parameters r . These functions control the smooth switch from the resummed prediction to the fixed-order result at large kinematic values.

(figures 8(a) and 8(c)), we show the absolute cross sections obtained using the modified additive matching scheme.

In the right panels (figures 8(b) and (d)), we compare the normalized shapes of our parton-level analytical predictions (NNLL matched to LO) with results from PYTHIA 8. The theoretical uncertainty bands incorporate the resummation and fixed-order scale variations, along with the sensitivity to the transition parameter r , combined in quadrature. These bands illustrate the stability of the matching procedure across the transition from the resummation-dominated region to the fixed-order tail. To evaluate non-perturbative effects, the PYTHIA 8 results are shown at the parton level (yellow), hadron level (red), and hadron level with multi-parton interactions (MPI) (grey).

For the azimuthal decorrelation $\delta\phi$, the NNLL+LO calculation agrees well with the Monte Carlo results at small $\delta\phi$. At large $\delta\phi$, the observed deviations are expected and

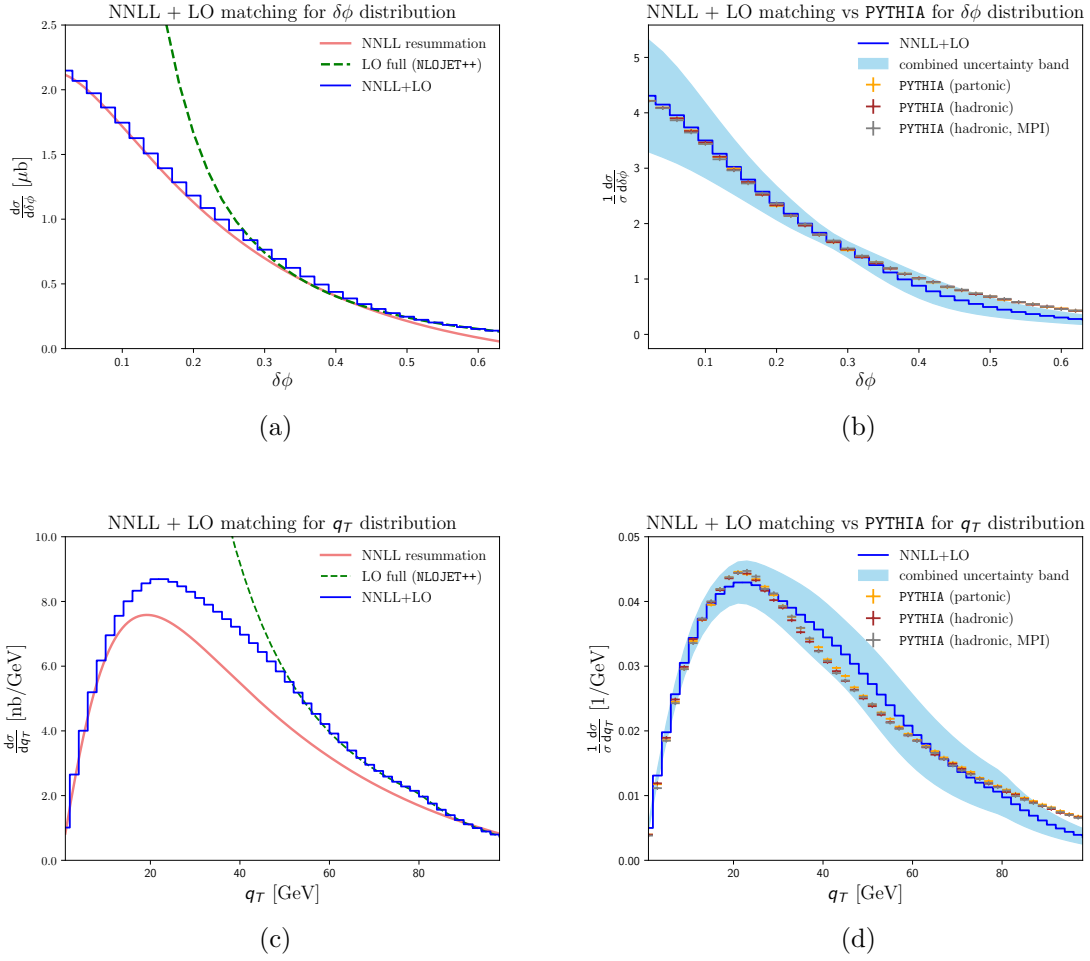


Figure 8: Matched distributions and comparison to PYTHIA. The kinematic cuts imposed on the jets are summarized in eq. (5.1). The top row displays the azimuthal decorrelation $\delta\phi$ (using transition parameter $r = 0.18$), while the bottom row displays the transverse momentum imbalance q_T ($r = 25$ GeV). The left column (a, c) shows the absolute differential cross sections. The right column (b, d) compares the shapes to PYTHIA results, with curves normalized to unity in the ranges $\delta\phi \in [0, 0.45]$ and $q_T \in [0, 30]$ GeV, respectively. The total uncertainty bands include contributions from resummation scale variations, fixed-order scale variations, and the transition parameter r , added in quadrature.

primarily driven by the absence of matching in PYTHIA. Furthermore, the three PYTHIA 8 predictions are nearly identical, indicating that $\delta\phi$ is largely insensitive to hadronization and MPI in this kinematic regime.

A similar behavior is observed for the q_T distribution (figure 8(d)), where the analytic predictions are consistent with PYTHIA 8, and the Monte Carlo results fall well within the theoretical uncertainty bands. As with $\delta\phi$, the non-perturbative corrections in PYTHIA 8 remain negligible. This confirms that for the chosen jet radius and kinematic cuts, the distribution is dominated by perturbative physics and is accurately captured by our re-

summation framework.

6 Conclusions

In this work, we have presented a comprehensive study of the azimuthal decorrelation $\delta\phi$ and the transverse momentum imbalance q_T in inclusive dijet production at the LHC. A central feature of our analysis is the use of the winner-take-all (WTA) recombination scheme for defining the jet axes. By adopting the WTA scheme, we eliminate the NGLs that plague standard jet definitions, thereby simplifying the all-order structure of the cross section.

We derived the factorization formulae for both observables using SCET. We demonstrated that, despite the common goal of measuring back-to-back kinematics, $\delta\phi$ and q_T exhibit distinct factorization structures. A particularly intricate aspect of our analysis was the treatment of the q_T distribution in the small jet radius limit ($R \ll 1$). We showed that the soft function requires a further refactorization into global soft, collinear-soft, and ultra-collinear-soft modes. Although the WTA scheme removes the standard NGLs of q_T , there are NGLs of R . Correspondingly, the scale hierarchy between collinear-soft and ultra-collinear-soft modes yields the non-trivial NGL evolution structure.

Numerically, we matched our resummed predictions to fixed-order LO calculations. For the azimuthal decorrelation $\delta\phi$, we achieved full NNLL accuracy. For the transverse momentum imbalance q_T , we implemented a joint resummation involving NNLL accuracy for global logarithms and LL accuracy for the small- R NGLs. Compared to NLL, our higher-order accuracy results in a substantial reduction of theoretical uncertainties. Our numerical analysis confirms that the scale-variation bands at NNLL (combined with LL accuracy for NGLs for q_T) lie consistently within the lower-order envelopes, indicating the robust convergence of our perturbative framework.

Finally, studies with PYTHIA 8 show that both the azimuthal decorrelation $\delta\phi$ and the transverse momentum imbalance q_T are robust against hadronization and multi-parton interactions. The agreement with our predictions is good; the primary discrepancies likely arise from the fixed-order matching, which is included in our calculations but absent in PYTHIA.

Our formalism provides a precise theoretical tool for probing the dynamics of QCD radiation in jet production at the LHC. The techniques developed here, particularly the handling of small- R refactorization and logarithmic power corrections, are applicable to a wide class of jet substructure observables and can facilitate future extractions of transverse-momentum-dependent (TMD) distributions.

Acknowledgments

R.J.F. and D.Y.S. are supported by the National Science Foundations of China under Grant No. 12275052, No. 12147101, No. 12547102. D.Y.S. is also supported by the Innovation Program for Quantum Science and Technology under grant No. 2024ZD0300101.

R.R. is supported by the European Union’s Horizon Europe research and innovation programme under the Marie Skłodowska-Curie project “SoftSERVE-NGL” with grant agreement No. 101108359. B.W. is supported by the Ramón y Cajal program with the Grant No. RYC2021-032271-I, the Xunta de Galicia under the ED431F 2023/10 project, the European Research Council project ERC-2018-ADG-835105 YoctoLHC, the project María de Maeztu CEX2023-001318-M financed by MCIN/AEI/10.13039/501100011033, by European Union ERDF, and by the Spanish Research State Agency under project PID2020-119632GBI00 and PID2023-152762NB-I00.

A NLO global soft functions

We choose a reference frame in which the zx -plane coincides with the scattering plane, and the beam ($i = a, b$) and jet ($i = 1, 2$) directions are specified by

$$\begin{aligned} n_a^\mu &= (1, 0, 0, 1), & n_b^\mu &= (1, 0, 0, -1), \\ n_1^\mu &= (1, \operatorname{sech} \eta_1, 0, \tanh \eta_1), & n_2^\mu &= (1, -\operatorname{sech} \eta_2, 0, \tanh \eta_2). \end{aligned}$$

Since at Born level the two jets are produced back-to-back in the transverse plane, their azimuthal angles can be fixed to $\phi_1 = 0$ and $\phi_2 = \pi$. The measurement 4-vector for q_T corresponds to $b^\mu = (0, \vec{b}_T, 0) = (0, b_T \cos \phi_b, b_T \sin \phi_b, 0)$ in impact-parameter space.

As discussed in section 3.3, the q_T soft function can be refactorized into global soft, collinear-soft, and ultra-collinear-soft contributions. In this appendix we present the explicit expression for the bare global-soft function at one loop level,

$$\mathbf{S}_{ijkl}^{\text{global}}(\vec{b}_T, \eta_1, \eta_2, \epsilon, \eta) = \sum_{i < j} (-\mathbf{T}_i \cdot \mathbf{T}_j) \omega_{ij}^{\text{global}}(\vec{b}_T, \eta_1, \eta_2, \epsilon, \eta) + \mathcal{O}(\alpha_s^2), \quad (\text{A.1})$$

where ϵ comes from dimensional regularization, and η is the rapidity regulator. Throughout this work, we use the $\overline{\text{MS}}$ renormalization scheme,

$$g_{s,0}^2 = 4\pi \left(\frac{\mu^2 e^{\gamma_E}}{4\pi} \right)^\epsilon \alpha_s(\mu) Z_\alpha, \quad Z_\alpha = 1 - \frac{\alpha_s(\mu) \beta_0}{4\pi \epsilon} + \mathcal{O}(\alpha_s^2). \quad (\text{A.2})$$

The NLO dipole contributing to the soft function can be written as

$$\omega_{ij}^{\text{global}}(\vec{b}_T, \eta_1, \eta_2, \epsilon, \eta) = \frac{\alpha_s(\mu) \mu^{2\epsilon} \pi^\epsilon e^{\gamma_E \epsilon}}{\pi^2} \int d^d k \delta(k^2) \theta(k^0) \omega^2 \left(\frac{\nu}{2k^0} \right)^\eta \frac{n_i \cdot n_j}{n_i \cdot k n_j \cdot k} e^{i\vec{k}_T \cdot \vec{b}_T}, \quad (\text{A.3})$$

where the factor $[\nu/(2k^0)]^\eta$ regulates the rapidity divergence that arises when the dipole involves an initial-state leg, i.e., for the beam–beam and beam–jet dipoles. The auxiliary bookkeeping parameter ω , introduced alongside the rapidity regulator, satisfies [102]

$$\frac{d}{d\nu} \omega = -\frac{\eta}{2} \omega, \quad \lim_{\eta \rightarrow 0} \omega \rightarrow 1, \quad (\text{A.4})$$

and ensures that the bare soft functions remain independent of the rapidity scale, in close analogy to the role of the renormalized coupling constant. After first expanding around $\eta \rightarrow 0$ and subsequently around $\epsilon \rightarrow 0$, the NLO beam-beam soft dipole is given by

$$\omega_{ab}^{\text{global}}(\vec{b}_T, \epsilon, \eta) = \frac{\alpha_s(\mu)}{4\pi} \left[\frac{4}{\epsilon^2} + 4 \left(\ln \frac{\mu^2}{\nu^2} - \frac{2}{\eta} \right) \left(\frac{1}{\epsilon} + \ln \frac{\mu^2 b_T^2}{b_0^2} \right) - 2 \ln^2 \frac{\mu^2 b_T^2}{b_0^2} - \frac{\pi^2}{3} \right]. \quad (\text{A.5})$$

The beam-jet dipole, with $i \in \{a, b\}$ and $j \in \{1, 2\}$, takes the form

$$\omega_{ij}^{\text{global}}(\vec{b}_T, \eta_j, \epsilon, \eta) = \frac{\alpha_s(\mu)}{4\pi} \left\{ 4 \left[-\frac{1}{\eta} + \ln \frac{\mu}{\nu} + \text{Sign}(n_{i,x}) \eta_j + \ln(-2i \cos(\phi_b - \phi_j)) \right] \right. \\ \left. \times \left(\frac{1}{\epsilon} + \ln \frac{\mu^2 b_T^2}{b_0^2} \right) + \frac{4}{\epsilon^2} + \frac{2}{\epsilon} \ln \frac{\mu^2 b_T^2}{b_0^2} - \frac{\pi^2}{3} \right\}. \quad (\text{A.6})$$

The global soft function for the jet-jet dipole has already been derived in ref. [103] and is free from rapidity divergences, yielding

$$\omega_{12}^{\text{global}}(\vec{b}_T, \eta_1, \eta_2, \epsilon) = \frac{\alpha_s(\mu) \mu^{2\epsilon} e^{\epsilon\gamma_E} B^\epsilon}{\pi} \Gamma(-\epsilon) \left[\Gamma(-\epsilon) \Gamma(1+\epsilon) \left(\frac{1+A_b}{-A_b} \right)^\epsilon \right. \\ \left. - \frac{\Gamma(-1-\epsilon)}{\Gamma(-\epsilon)} A_b {}_2F_1(1, 1, 2+\epsilon, -A_b) \right] \\ = \frac{\alpha_s(\mu)}{4\pi} \left\{ \frac{4}{\epsilon^2} + \frac{4}{\epsilon} \left[\ln \frac{\mu^2 b_0^2}{b_T^2} - \ln(-A_b) \right] + 2 \ln^2 \frac{\mu^2 b_0^2}{b_T^2} - 4 \ln(-A_b) \ln \frac{\mu^2 b_0^2}{b_T^2} \right. \\ \left. + 2 \ln^2(-A_b) - 4 \ln(-A_b) \ln(1+A_b) - 4 \text{Li}_2(-A_b) + \pi^2 \right\}, \quad (\text{A.7})$$

with the shorthand notation

$$A_b \equiv \frac{b_T^2 (n_1 \cdot n_2)}{2(n_1 \cdot b)(n_2 \cdot b)} = -\frac{\hat{s}}{4p_T^2 \cos^2 \phi_b} = -\frac{1 + \cosh(\eta_1 - \eta_2)}{2 \cos^2 \phi_b}, \quad B \equiv \frac{|\vec{b}_T|^2}{4}. \quad (\text{A.8})$$

B Collinear-soft and ultra-collinear-soft functions up to NNLO

In this appendix, we present the explicit bare expression for S_i defined in eq. (3.26), which combines the collinear-soft and ultra-collinear-soft contributions, up to NNLO accuracy.

Following eqs. (3.31) and (3.33), the b -parameter dependence of S_i can be reorganized as

$$S_i(b_\perp, b^+) = 1 + \frac{Z_\alpha \alpha_s(\mu)}{4\pi} S_i^{(1)}(b_\perp, b^+) + \left(\frac{Z_\alpha \alpha_s(\mu)}{4\pi} \right)^2 S_i^{(2)}(b_\perp, b^+) + \mathcal{O}(\alpha_s^3), \quad (\text{B.1})$$

where $b_\perp = b_y = b_T \sin \phi_b$, and

$$b^+ = b \cdot n_i = \begin{cases} -b_T \cos \phi_b \text{sech } \eta_1, & i = 1 \\ b_T \cos \phi_b \text{sech } \eta_2, & i = 2 \end{cases}.$$

For brevity, we suppress several nonessential arguments in the notation for S_i and for the collinear-soft and ultra-collinear-soft functions introduced below, including the regulators ϵ and η , the jet radius R , and the dependence on $\{n_i, \bar{n}_i, \mathbf{u}\}$.

We begin with the NLO expression,

$$\begin{aligned} S_i^{(1)}(b_\perp, b^+) &= \langle \mathbf{S}_0^{\text{ucs}(0)} \mathbf{S}_0^{\text{cs}(1)} \rangle + \langle \mathbf{S}_0^{\text{ucs}(1)} \mathbf{S}_0^{\text{cs}(0)} \rangle + \langle \mathbf{S}_1^{\text{ucs}(0)} \otimes \mathbf{S}_1^{\text{cs}(1)} \rangle \\ &= \langle \mathbf{S}_0^{\text{ucs}(1)} \rangle + \langle \mathbf{1} \otimes \mathbf{S}_1^{\text{cs}(1)} \rangle, \end{aligned} \quad (\text{B.2})$$

where the superscripts (0) and (1) denote the perturbative order of the collinear-soft and ultra-collinear-soft functions. Note that the *subscripts* 0 and 1 here denote the relevant values for m_i contributing at NLO and are unrelated to the perturbative order or the index i . The dependence on the index i is hidden, on the RHS, in the suppressed arguments for the collinear-soft and ultra-collinear-soft functions. Only the tree-level contribution of $\mathbf{S}_1^{\text{ucs}}$ is needed at NLO, as shown in eq. (B.2), because $\mathbf{S}_{m_i}^{\text{cs}} \sim \mathcal{O}(\alpha_s^{m_i})$. The second equality in eq. (B.2) follows from $\mathbf{S}_1^{\text{ucs}} = \mathbf{1} + \mathcal{O}(\alpha_s)$ and $\mathbf{S}_0^{\text{cs}} = \mathbf{1}$. Since no additional collinear parton directions are integrated over, we omit the $\otimes \mathbf{S}_0^{\text{cs}}$ term inside the color trace.

The explicit NLO expressions for the collinear-soft and ultra-collinear-soft functions are

$$\langle \mathbf{1} \otimes \mathbf{S}_1^{\text{cs}(1)}(b_\perp) \rangle = C_i \left(\frac{\mu|b_\perp|}{b_0} \right)^{2\epsilon} \left(\frac{\nu|b_\perp|R_i}{b_0} \right)^\eta h_{\text{in}}, \quad \langle \mathbf{S}_0^{\text{ucs}(1)}(b^+) \rangle = C_i \left(\frac{i b^+ \mu}{b_0 R_i} \right)^{2\epsilon} s_{\text{out}}, \quad (\text{B.3})$$

where $b_0 = 2e^{-\gamma_E}$, $R_i = R/(2 \cosh \eta_i)$, and

$$\begin{aligned} h_{\text{in}} &= \frac{2}{\epsilon^2} - \frac{4}{\eta\epsilon} - \frac{\pi^2}{6} + \left(-\frac{\eta}{\epsilon^3} + \frac{\pi^2\eta}{12\epsilon} - \frac{\zeta_3}{3}\eta - \frac{\pi^2\epsilon}{3\eta} - \frac{4\zeta_3}{3}\epsilon - \frac{17\pi^4}{1440}\eta\epsilon \right. \\ &\quad \left. - \frac{4\zeta_3\epsilon^2}{3\eta} - \frac{3\pi^4}{80}\epsilon^2 - \frac{\pi^4\epsilon^3}{40\eta} \right), \end{aligned} \quad (\text{B.4})$$

$$s_{\text{out}} = -\frac{2}{\epsilon^2} - \frac{\pi^2}{2} + \left(-\frac{14\zeta_3}{3}\epsilon - \frac{7\pi^4}{48}\epsilon^2 \right). \quad (\text{B.5})$$

Applying similar simplifications as in eq. (B.2), one can obtain the NNLO expression of the combination of collinear-soft and ultra-collinear-soft functions,

$$S_i^{(2)}(b_\perp, b^+) = \langle \mathbf{1} \otimes \mathbf{S}_1^{\text{cs}(2)} \rangle + \langle \mathbf{1} \otimes \mathbf{S}_2^{\text{cs}(2)} \rangle + \langle \mathbf{S}_0^{\text{ucs}(2)} \rangle + \langle \mathbf{S}_1^{\text{ucs}(1)} \otimes \mathbf{S}_1^{\text{cs}(1)} \rangle. \quad (\text{B.6})$$

The first two terms arise purely from the collinear-soft sector. They consist of a real-virtual contribution $\langle \mathbf{1} \otimes \mathbf{S}_1^{\text{cs}(2)} \rangle$ and a double-real emission contribution $\langle \mathbf{1} \otimes \mathbf{S}_2^{\text{cs}(2)} \rangle$, with all the collinear-soft real emissions constrained to lie inside the jet cone,

$$\begin{aligned} \langle \mathbf{1} \otimes \mathbf{S}_1^{\text{cs}(2)}(b_\perp) \rangle &= \left(\frac{\mu|b_\perp|}{b_0} \right)^{4\epsilon} \left(\frac{\nu|b_\perp|R_i}{b_0} \right)^\eta \omega^2 C_i C_A v_A^{\text{in}}, \\ \langle \mathbf{1} \otimes \mathbf{S}_2^{\text{cs}(2)}(b_\perp) \rangle &= \left(\frac{\mu|b_\perp|}{b_0} \right)^{4\epsilon} \left(\frac{\nu|b_\perp|R_i}{b_0} \right)^\eta \omega^2 \left[\omega^2 \left(\frac{\nu|b_\perp|R_i}{b_0} \right)^\eta C_i^2 \frac{h_{\text{in}}^2}{2} \right. \end{aligned} \quad (\text{B.7})$$

$$+ C_i C_A h_A + C_i n_f T_F h_f \Big]. \quad (\text{B.8})$$

The coefficients v_A^{in} , $h_{\text{in}}^2/2$, h_A and h_f can be computed using the parametrization in ref. [104],

$$v_A^{\text{in}} = -\frac{1}{\epsilon^4} + \frac{4}{\eta\epsilon^3} + \frac{\pi^2}{2} \frac{1}{\epsilon^2} - \frac{2\pi^2}{3} \frac{1}{\eta\epsilon} + \frac{28\zeta_3}{3} \frac{1}{\epsilon} + \frac{8\zeta_3}{3} \frac{1}{\eta} + \frac{19\pi^4}{120}, \quad (\text{B.9})$$

$$\frac{h_{\text{in}}^2}{2} = \frac{6}{\epsilon^4} - \frac{8}{\eta\epsilon^3} + \left(\frac{8}{\eta^2} - \frac{\pi^2}{3}\right) \frac{1}{\epsilon^2} + \frac{4\pi^2}{3\eta^2} + \frac{8\zeta_3}{3\eta} - \frac{\pi^4}{60}, \quad (\text{B.10})$$

$$h_A = \frac{1}{\epsilon^4} - \frac{4}{\eta\epsilon^3} + \frac{11}{6\epsilon^3} - \frac{22}{3\eta\epsilon^2} + \left(\frac{67}{18} - \pi^2\right) \frac{1}{\epsilon^2} + \left(-\frac{134}{9} + \frac{4\pi^2}{3}\right) \frac{1}{\eta\epsilon} \\ + \left(\frac{211}{27} - \frac{77\pi^2}{36} - \frac{61\zeta_3}{3}\right) \frac{1}{\epsilon} + \left(-\frac{808}{27} - \frac{11\pi^2}{9} + \frac{76\zeta_3}{3}\right) \frac{1}{\eta} - 65.260(36), \quad (\text{B.11})$$

$$h_f = -\frac{2}{3\epsilon^3} + \frac{8}{3\eta\epsilon^2} - \frac{10}{9\epsilon^2} + \frac{40}{9\eta\epsilon} + \left(-\frac{74}{27} + \frac{7\pi^2}{9}\right) \frac{1}{\epsilon} + \left(\frac{224}{27} + \frac{4\pi^2}{9}\right) \frac{1}{\eta} + 24.72953(77). \quad (\text{B.12})$$

The pure ultra-collinear-soft contribution takes the form

$$\langle \mathcal{S}_0^{\text{ucs}(2)}(b^+) \rangle = \left(\frac{ib^+\mu}{b_0 R_i}\right)^{4\epsilon} \left[C_i^2 \frac{s_{\text{out}}^2}{2} + C_i C_A s_A + C_i n_f T_F s_f \right], \quad (\text{B.13})$$

with

$$\frac{s_{\text{out}}^2}{2} = \frac{2}{\epsilon^4} + \frac{\pi^2}{\epsilon^2} + \frac{28\zeta_3}{3\epsilon} + \frac{5\pi^4}{12}. \quad (\text{B.14})$$

While the collinear-soft radiation is confined within the jet cone, the ultra-collinear-soft partons are unconstrained by the jet boundary and can be emitted both inside and outside the jet. However, only the out-of-cone ultra-collinear-soft momentum is measured, which leads to a further decomposition of the coefficients s_A and s_f as

$$s_A \equiv g_A + v_A^{\text{out}} + q_A, \quad s_f \equiv g_f + q_f. \quad (\text{B.15})$$

The terms g_A and g_f denote the double-real emission contributions where both ultra-collinear-soft partons are radiated outside the jet cone and are therefore fully measured. These evaluate to

$$g_A = -\frac{1}{\epsilon^4} - \frac{11}{6\epsilon^3} + \left(-\frac{67}{18} - \pi^2\right) \frac{1}{\epsilon^2} + \left(-\frac{193}{27} - \frac{11\pi^2}{4} - \frac{35\zeta_3}{3}\right) \frac{1}{\epsilon} \\ + \left(-\frac{1196}{81} - \frac{67\pi^2}{12} - \frac{31\pi^4}{40} - \frac{473\zeta_3}{9}\right), \quad (\text{B.16})$$

$$g_f = \frac{2}{3\epsilon^3} + \frac{10}{9\epsilon^2} + \left(\frac{38}{27} + \pi^2\right) \frac{1}{\epsilon} + \left(\frac{238}{81} + \frac{5\pi^2}{3} + \frac{172\zeta_3}{9}\right). \quad (\text{B.17})$$

The term v_A^{out} in eq. (B.15) corresponds to the real-virtual correction with the single ultra-collinear-soft gluon radiated outside the jet cone, yielding

$$v_A^{\text{out}} = \frac{1}{\epsilon^4} + \frac{5\pi^2}{6} \frac{1}{\epsilon^2} + \frac{56\zeta_3}{3} \frac{1}{\epsilon} + \frac{113\pi^4}{120}. \quad (\text{B.18})$$

Explicit forms of g_A , g_f and v_A^{out} can also be extracted from the hemisphere soft function in ref. [105]. The quantities q_f and q_A in eq. (B.15) describe the double-real contributions in which one ultra-collinear-soft emission lies inside the jet cone and is unobserved, while the other is emitted outside the jet cone and measured,

$$q_A = \left(-\frac{2}{3} + \frac{22\pi^2}{9} - 4\zeta_3 \right) \frac{1}{\epsilon} + \frac{40}{9} - \frac{134\pi^2}{27} + \frac{44\zeta_3}{3} + \frac{8\pi^4}{45}, \quad (\text{B.19})$$

$$q_f = \left(\frac{4}{3} - \frac{8\pi^2}{9} \right) \frac{1}{\epsilon} - \frac{68}{9} + \frac{64\pi^2}{27} - \frac{16\zeta_3}{3}. \quad (\text{B.20})$$

The opposite-side NNLO contribution with different modes is obtained through the convolution between the NLO collinear-soft and NLO ultra-collinear-soft functions,

$$\langle \mathbf{S}_1^{\text{ucs}(1)} \otimes \mathbf{S}_1^{\text{cs}(1)} \rangle = \left(\frac{\mu|b_\perp|}{b_0} \right)^{2\epsilon} \left(\frac{ib^+\mu}{b_0 R_i} \right)^{2\epsilon} \left[\left(\frac{\nu|b_\perp|R_i}{b_0} \right)^\eta \omega^2 C_i^2 p_{2i} + C_i C_{AP_A} \right], \quad (\text{B.21})$$

with

$$p_{2i} = h_{\text{in}S_{\text{out}}} = -\frac{4}{\epsilon^4} + \frac{8}{\eta\epsilon^3} - \frac{2\pi^2}{3\epsilon^2} + \frac{8\pi^2}{3\eta\epsilon} - \frac{20\zeta_3}{3\epsilon} + \frac{64\zeta_3}{3\eta} - \frac{2\pi^4}{15}, \quad (\text{B.22})$$

$$p_A = \frac{2\pi^2}{3\epsilon^2} + \frac{8\zeta_3}{\epsilon} + \frac{23\pi^4}{45}. \quad (\text{B.23})$$

Combining these pieces, the NNLO contribution to S_i , defined in eq. (3.26), can be organized as

$$\begin{aligned} S_i^{(2)}(b_\perp, b^+) &= \left(\frac{\mu|b_\perp|}{b_0} \right)^{4\epsilon} \left(\frac{\nu|b_\perp|R_i}{b_0} \right)^\eta \omega^2 \left[\omega^2 \left(\frac{\nu|b_\perp|R_i}{b_0} \right)^\eta C_i^2 \frac{h_{\text{in}}^2}{2} \right. \\ &\quad \left. + C_i C_A (h_A + v_A^{\text{in}}) + C_i n_f T_F h_f \right] \\ &\quad + \left(\frac{ib^+\mu}{b_0 R_i} \right)^{4\epsilon} \left[C_i^2 \frac{s_{\text{out}}^2}{2} + C_i C_A (g_A + v_A^{\text{out}}) + C_i n_f T_F g_f \right] \\ &\quad + \left(\frac{ib^+\mu}{b_0 R_i} \right)^{4\epsilon} \left[C_i C_A (s_A - g_A - v_A^{\text{out}}) + C_i n_f T_F (s_f - g_f) \right] \\ &\quad + \left(\frac{\mu|b_\perp|}{b_0} \right)^{2\epsilon} \left(\frac{ib^+\mu}{b_0 R_i} \right)^{2\epsilon} \left[\left(\frac{\nu|b_\perp|R_i}{b_0} \right)^\eta \omega^2 C_i^2 h_{\text{in}S_{\text{out}}} + C_i C_{AP_A} \right]. \quad (\text{B.24}) \end{aligned}$$

B.1 Renormalization and anomalous dimensions in multiplicity space

Due to the restricted phase space in the collinear-soft function, non-global logarithms (NGLs) arise in the calculation of the collinear-soft and ultra-collinear-soft functions. As

discussed in [36, 85], both global and non-global large logarithms can be resummed through the RG evolution of these functions.

However, part of the infrared divergence in the collinear-soft function should be removed by the collinear-soft function with lower parton multiplicity, which means its renormalization constant is a matrix in multiplicity space,

$$\mathcal{S}_m^{\text{CS}}(\{n_i, \bar{n}_i, \underline{u}\}, b_y, R, \epsilon, \eta) = \sum_{l=0}^m \mathbf{Z}_{ml}^{\text{CS}}(\{n_i, \bar{n}_i, \underline{u}\}, b_y, R, \epsilon, \eta, \mu, \nu) \mathcal{S}_l^{\text{CS}}(\{n_i, \bar{n}_i, \underline{u}\}, b_y, R, \mu, \nu), \quad (\text{B.25})$$

where we suppress the subscript i on the multiplicity indices m_i and l_i for notational simplicity, a convention we maintain hereafter. In this equation, the renormalization constant \mathbf{Z}^{CS} is a lower-triangular matrix in multiplicity space. This differs slightly from the notation used in refs. [36, 85], as we organize the expression such that \mathbf{Z}^{CS} multiplies the renormalized collinear-soft function from the left, equating to the bare collinear-soft function, rather than multiplying from the right. Moreover, although eq. (B.25) includes the renormalization of rapidity divergences, the rapidity evolution is trivial and does not induce mixing between collinear-soft functions of different multiplicities. Thus, we can further decompose $\mathbf{Z}_{ml}^{\text{CS}}$ into an overall factor Z^{CS} and a multiplicity-mixing matrix contribution $\hat{\mathbf{Z}}_{ml}$, according to

$$\mathbf{Z}_{ml}^{\text{CS}}(\{n_i, \bar{n}_i, \underline{u}\}, b_y, R, \epsilon, \eta, \mu, \nu) = Z^{\text{CS}}(\{n_i, \bar{n}_i\}, b_y, R, \epsilon, \eta, \mu, \nu) \hat{\mathbf{Z}}_{ml}(\{n_i, \bar{n}_i, \underline{u}\}, \epsilon, \mu). \quad (\text{B.26})$$

Similarly, the ultra-collinear-soft function can be renormalized using a lower-triangular renormalization constant \mathbf{Z}^{UCS} ,

$$\mathcal{S}_l^{\text{UCS}}(\{n_i, \bar{n}_i, \underline{u}\}, b_x, R, \mu) = \sum_{m=l}^{\infty} \mathcal{S}_m^{\text{UCS}}(\{n_i, \bar{n}_i, \underline{u}\}, b_x, R, \epsilon) \hat{\otimes} \mathbf{Z}_{ml}^{\text{UCS}}(\{n_i, \bar{n}_i, \underline{u}\}, b_x, R, \epsilon, \mu), \quad (\text{B.27})$$

which implies that higher-multiplicity ultra-collinear-soft functions are required to absorb the divergences of the lower-multiplicity ones. The symbol $\hat{\otimes}$ indicates that an integration must be performed over the additional $(m - l)$ directions of the collinear-soft partons on which the bare function $\mathcal{S}_m^{\text{UCS}}(\{n_i, \bar{n}_i, \underline{u}\}, b_x, R, \epsilon)$ depends. The renormalization constant for the ultra-collinear-soft function can likewise be decomposed into two parts,

$$\mathbf{Z}_{ml}^{\text{UCS}}(\{n_i, \bar{n}_i, \underline{u}\}, b_x, R, \epsilon, \mu) = \frac{\hat{\mathbf{Z}}_{ml}(\{n_i, \bar{n}_i, \underline{u}\}, \epsilon, \mu)}{Z^{\text{UCS}}(\{n_i, \bar{n}_i\}, b_x, R, \epsilon, \mu)}. \quad (\text{B.28})$$

Since the multiplicity mixing in the RG evolution occurs only between the collinear-soft and ultra-collinear-soft functions, the lower-triangular matrices $\hat{\mathbf{Z}}_{ml}$ in eqs. (B.26) and (B.28) are identical and independent from the b -dependence.

Next, we derive the anomalous dimensions and RG equations for the collinear-soft and ultra-collinear-soft functions. The anomalous dimensions can be obtained directly from their corresponding renormalization constants. If the renormalization constant is a scalar, one has

$$\Gamma = - \lim_{\epsilon \rightarrow 0} Z^{-1}(\epsilon, \mu) \frac{d}{d \ln \mu} Z(\epsilon, \mu), \quad (\text{B.29})$$

where $\Gamma \in \{\Gamma^{\text{cs}}, \Gamma^{\text{ucs}}\}$ and $Z \in \{Z^{\text{cs}}, Z^{\text{ucs}}\}$. If the renormalization constant is a matrix in multiplicity space, the anomalous dimensions can be obtained from the following relation

$$\frac{d}{d \ln \mu} \mathbf{Z}_{ml}(\epsilon, \mu) = - \sum_{k=l}^m \mathbf{Z}_{mk}(\epsilon, \mu) \mathbf{\Gamma}_{kl}(\mu), \quad (\text{B.30})$$

where $\mathbf{\Gamma}_{kl} \in \{\mathbf{\Gamma}_{kl}^{\text{cs}}, \mathbf{\Gamma}_{kl}^{\text{ucs}}, \hat{\mathbf{\Gamma}}_{kl}\}$ and $\mathbf{Z}_{mk} \in \{\mathbf{Z}_{mk}^{\text{cs}}, \mathbf{Z}_{mk}^{\text{ucs}}, \hat{\mathbf{Z}}_{mk}\}$.

Therefore, the standard form of the RG equations can be derived as,

$$\begin{aligned} \frac{d}{d \ln \mu} \mathbf{S}_m^{\text{cs}}(\{n_i, \bar{n}_i, \underline{u}\}, b_y, R, \mu, \nu) &= \sum_{l=0}^m \mathbf{\Gamma}_{ml}^{\text{cs}} \mathbf{S}_l^{\text{cs}}(\{n_i, \bar{n}_i, \underline{u}\}, b_y, R, \mu, \nu) \\ &= \sum_{l=0}^m \left(\mathbf{\Gamma}_{ml}^{\text{cs}} \mathbf{1} + \hat{\mathbf{\Gamma}}_{ml} \right) \mathbf{S}_l^{\text{cs}}(\{n_i, \bar{n}_i, \underline{u}\}, b_y, R, \mu, \nu), \end{aligned} \quad (\text{B.31})$$

$$\begin{aligned} \frac{d}{d \ln \mu} \mathbf{S}_l^{\text{ucs}}(\{n_i, \bar{n}_i, \underline{u}\}, b_x, R, \mu) &= - \sum_{m=l}^{\infty} \mathbf{S}_m^{\text{ucs}}(\{n_i, \bar{n}_i, \underline{u}\}, b_x, R, \mu) \hat{\otimes} \mathbf{\Gamma}_{ml}^{\text{ucs}} \\ &= \sum_{m=l}^{\infty} \mathbf{S}_m^{\text{ucs}}(\{n_i, \bar{n}_i, \underline{u}\}, b_x, R, \mu) \hat{\otimes} \left(\mathbf{\Gamma}_{ml}^{\text{ucs}} \mathbf{1} - \hat{\mathbf{\Gamma}}_{ml} \right). \end{aligned} \quad (\text{B.32})$$

The second equality follows from separating the overall and multiplicity-mixing anomalous dimensions. Since the multiplicity-mixing contributions in the RG evolution of the collinear-soft and ultra-collinear-soft functions cancel each other, their combination S_i , defined in eq. (3.26), evolves under the RG without any residual multiplicity mixing,

$$\frac{d}{d \ln \mu} S_i(\vec{b}_T, \eta_i, R, \mu, \nu) = (\mathbf{\Gamma}^{\text{cs}} + \mathbf{\Gamma}^{\text{ucs}}) S_i(\vec{b}_T, \eta_i, R, \mu, \nu). \quad (\text{B.33})$$

Based on the explicit NNLO expressions in appendix B, the two-loop global anomalous dimensions for the collinear-soft and ultra-collinear-soft functions are

$$\mathbf{\Gamma}^{\text{cs}}(\alpha_s, \{n_i, \bar{n}_i\}, R, \mu, \nu) = 2C_i \gamma_{\text{cusp}}(\alpha_s) \ln \frac{\mu}{\nu R_i}, \quad (\text{B.34})$$

$$\mathbf{\Gamma}^{\text{ucs}}(\alpha_s, \{n_i, \bar{n}_i\}, b_x, R, \mu) = -C_i \gamma_{\text{cusp}}(\alpha_s) \left[\ln \frac{4\mu^2 b_x^2}{b_0^2 R^2} - i\pi \text{Sign}(b_x n_{i,x}) \right], \quad (\text{B.35})$$

with $L_b = \ln(\mu^2 b_T^2 / b_0^2) = \ln(\mu^2 b_T^2 e^{2\gamma_E} / 4)$. The treatment of the matrix-valued anomalous dimension $\hat{\mathbf{\Gamma}}_{ml}$ and the final resummation of both global and NGLs is discussed in section 4.2.

$S_i(\vec{b}_T, \eta_i, R, \mu, \nu)$ also satisfies the following RRG equation,

$$\frac{d}{d \ln \nu} S_i(\vec{b}_T, \eta_i, R, \mu, \nu) = \mathbf{\Gamma}_{\nu}^{S_i} S_i(\vec{b}_T, \eta_i, R, \mu, \nu) \quad (\text{B.36})$$

where the rapidity anomalous dimension is given by $\mathbf{\Gamma}_{\nu}^{S_i} = -\mathbf{\Gamma}_{\nu}^i(b_y, \mu)$, with $\mathbf{\Gamma}_{\nu}^i(b_y, \mu)$ defined in eq. (3.15).

C Jet radius power corrections from hemisphere soft functions

In addition to the effective theory framework developed in [35, 36, 85], one can compute S_i in the small- R limit by treating it as a hemisphere soft function that is highly boosted along the jet direction n_i . Note that we are not referring to the standard hemisphere soft function for jet mass but include the measurements for our case, see eqs. (C.4) and (C.9). This allows us to assess the power corrections to the refactorization in terms of collinear-soft and ultra-collinear-soft functions.

Since the original Wilson lines n_i and \bar{n}_i are back-to-back, one can rotate them into the directions $n(n_a)$ and $\bar{n}(n_b)$ to simplify the calculations. Moreover, the integral definition of the boosted hemisphere soft function is invariant under this rotation.

C.1 Integral definition

The explicit form of the boosted hemisphere soft functions for the QCD leg labeled by parton i is given by

$$S_i^{\text{hemi}}(b_\perp, b^+) = 1 + \frac{Z_\alpha \alpha_s(\mu)}{4\pi} S_i^{\text{hemi},(1)}(b_\perp, b^+) + \left(\frac{Z_\alpha \alpha_s(\mu)}{4\pi} \right)^2 S_i^{\text{hemi},(2)}(b_\perp, b^+) + \mathcal{O}(\alpha_s^3). \quad (\text{C.1})$$

The single-real emission correction splits into two components,

$$S_i^{\text{hemi},(1)}(b_\perp, b^+) = S_i^{\text{in}}(b_\perp) + S_i^{\text{out}}(b^+), \quad (\text{C.2})$$

whose integral definitions are

$$S_i^{\text{in},\text{out}}(b) = 16\pi^2 \left(\frac{\mu^2 e^{\gamma_E}}{4\pi} \right)^\epsilon \int \frac{d^d k}{(2\pi)^{d-1}} \delta(k^2) \theta(k^0) \frac{4C_i}{k^- k^+} \mathcal{M}_1^{\text{in},\text{out}}(b). \quad (\text{C.3})$$

The corresponding measurement function $\mathcal{M}_1^{\text{in},\text{out}}$, together with the rapidity regulator (when needed), is given by

$$\mathcal{M}_1^{\text{in}}(b_\perp) = \left(\frac{\nu}{k^-} \right)^\alpha \theta \left(R_i^2 - \frac{k^+}{k^-} \right) e^{ik_y b_\perp}, \quad \mathcal{M}_1^{\text{out}}(b^+) = \theta \left(\frac{k^+}{k^-} - R_i^2 \right) e^{-i\frac{1}{2}k^- b^+}. \quad (\text{C.4})$$

Our NNLO hemisphere soft function is therefore,

$$S_i^{\text{hemi},(2)}(b_\perp, b^+) = S_{i,RR}(b_\perp, b^+) + S_{i,RV}^{\text{in}}(b_\perp) + S_{i,RV}^{\text{out}}(b^+), \quad (\text{C.5})$$

with the real-virtual correction given by

$$S_{i,RV}^{\text{in},\text{out}}(b) = 256\pi^4 \left(\frac{\mu^2 e^{\gamma_E}}{4\pi} \right)^{2\epsilon} \int \frac{d^d k}{(2\pi)^{d-1}} \delta(k^2) \theta(k^0) |\mathcal{A}_{RV}(k)|^2 \mathcal{M}_1^{\text{in},\text{out}}(b), \quad (\text{C.6})$$

involving the amplitude

$$|\mathcal{A}_{RV}(k)|^2 = -(4\pi)^\epsilon \frac{C_i C_A}{4(k^-)^{1+\epsilon} (k^+)^{1+\epsilon}} \frac{\Gamma(-\epsilon) \cot(\pi\epsilon)}{\Gamma(-2\epsilon) \sin(\pi\epsilon)}. \quad (\text{C.7})$$

The double-real correction is given by

$$S_{i,RR}(b_\perp, b^+) = 256\pi^4 \left(\frac{\mu^2 e^{\gamma_E}}{4\pi} \right)^{2\epsilon} \int \frac{d^d k}{(2\pi)^{d-1}} \delta(k^2) \theta(k^0) \int \frac{d^d q}{(2\pi)^{d-1}} \delta(q^2) \theta(q^0) \\ \times \sum_X |\mathcal{A}_{RR}^{(X)}(k, q)|^2 \mathcal{M}_2^{(X)}(k, q, b_\perp, b^+), \quad (\text{C.8})$$

where $X = C_i^2, C_i C_A, C_i n_f T_F$ denotes the color channel, and $\mathcal{M}_2(k, q, b_\perp, b^+)$ represents the measurement function combined with the Fourier factor,

$$\mathcal{M}_2^{(X)}(k, q, b_\perp, b^+) = \frac{1}{2!} \left[\left(\frac{\nu}{k^-} \right)^\eta \theta \left(R_j^2 - \frac{k^+}{k^-} \right) \theta \left(\frac{q^+}{q^-} - R_j^2 \right) e^{ik_y b_\perp - i\frac{1}{2} q^- b^+} \right. \\ + \left(\frac{\nu}{q^-} \right)^\eta \theta \left(\frac{k^+}{k^-} - R_j^2 \right) \theta \left(R_j^2 - \frac{q^+}{q^-} \right) e^{-i\frac{1}{2} k^- b^+ + i q_y b_\perp} \\ + R^{(X)}(\nu, \eta, k^-, q^-) \theta \left(R_j^2 - \frac{k^+}{k^-} \right) \theta \left(R_j^2 - \frac{q^+}{q^-} \right) e^{i(k_y + q_y) b_\perp} \\ \left. + \theta \left(\frac{k^+}{k^-} - R_j^2 \right) \theta \left(\frac{q^+}{q^-} - R_j^2 \right) e^{-i\frac{1}{2} (k^- + q^-) b^+} \right], \quad (\text{C.9})$$

where $R^{(X)}(\nu, \eta, k^-, q^-)$ denotes the rapidity regulator for the case in which both double-real emissions are radiated inside the jet. To derive the correct RG equations and to consistently combine the hemisphere soft functions with the jet functions, the rapidity regulator must be introduced at the level of connected webs [69]. Consequently, one needs to distinguish between the contributions from uncorrelated and correlated emissions, according to

$$R^{(X)}(\nu, \eta, k^-, q^-) = \begin{cases} (\nu/k^-)^\eta (\nu/q^-)^\eta, & X = C_i^2, \\ [\nu/(k^- + q^-)]^\eta, & X = C_i C_A \text{ or } C_i n_f T_F. \end{cases} \quad (\text{C.10})$$

The squared amplitudes read

$$|\mathcal{A}_{RR}^{(C_i^2)}(k, q)|^2 = \frac{16 C_i^2}{k^- k^+ q^- q^+}, \quad (\text{C.11})$$

$$|\mathcal{A}_{RR}^{(n_f)}(k, q)|^2 = 2! \times 2 C_i T_F n_f \frac{2k \cdot q (k^+ + q^+) (k^- + q^-) - (k^+ q^- - k^- q^+)^2}{(k^+ + q^+)^2 (k^- + q^-)^2 (k \cdot q)^2}, \quad (\text{C.12})$$

$$|\mathcal{A}_{RR}^{(C_A)}(k, q)|^2 = C_i C_A \left\{ -4 \frac{k^+ (2k^- + q^-) + q^+ (k^- + 2q^-)}{k^+ k^- q^+ q^- (k^+ + q^+) (k^- + q^-)} + \frac{2(1 - \epsilon) (k^- q^+ - q^- k^+)^2}{(k^+ + q^+)^2 (k^- + q^-)^2 (k \cdot q)^2} \right. \\ \left. + 2 \frac{(k^+)^2 q^- (2k^- + q^-) + 2k^+ q^+ ((k^-)^2 - k^- q^- + (q^-)^2) + k^- (q^+)^2 (k^- + 2q^-)}{k^+ k^- q^+ q^- (k^+ + q^+) (k^- + q^-) (k \cdot q)} \right\}. \quad (\text{C.13})$$

C.2 Boosted hemisphere soft functions

The NLO expression of the boosted hemisphere soft function coincides with the NLO result for S_i defined in eq. (B.3),

$$S_i^{\text{in}}(b_\perp) = C_i \left(\frac{\mu|b_\perp|}{b_0} \right)^{2\epsilon} \left(\frac{\nu|b_\perp|R_i}{b_0} \right)^\eta h_{\text{in}}, \quad S_i^{\text{out}}(b^+) = C_i \left(\frac{ib^+\mu}{b_0 R_i} \right)^{2\epsilon} s_{\text{out}}. \quad (\text{C.14})$$

The NNLO hemisphere soft function takes the following form,

$$\begin{aligned} S_i^{\text{hemi,(2)}}(b_\perp, b^+) &= \left(\frac{\mu|b_\perp|}{b_0} \right)^{4\epsilon} \left(\frac{\nu|b_\perp|R_i}{b_0} \right)^\eta \omega^2 \left[\omega^2 \left(\frac{\nu|b_\perp|R_i}{b_0} \right)^\eta C_i^2 \frac{h_{\text{in}}^2}{2} \right. \\ &\quad \left. + C_i C_A (h_A + v_A^{\text{in}}) + C_i n_f T_F h_f \right] \\ &\quad + \left(\frac{ib^+\mu}{b_0 R_i} \right)^{4\epsilon} \left[C_i^2 \frac{s_{\text{out}}^2}{2} + C_i C_A (g_A + v_A^{\text{out}}) + C_i n_f T_F g_f \right] \\ &\quad + \left(\frac{\mu|b_\perp|}{b_0} \right)^{2\epsilon} \left(\frac{ib^+\mu}{b_0 R_i} \right)^{2\epsilon} (C_i C_A r_A(r) + C_i n_f T_F r_f(r)) \\ &\quad + \left(\frac{\mu|b_\perp|}{b_0} \right)^{2\epsilon} \left(\frac{ib^+\mu}{b_0 R_i} \right)^{2\epsilon} \left(\frac{\nu|b_\perp|R_i}{b_0} \right)^\eta \omega^2 C_i^2 h_{\text{in}} s_{\text{out}}. \end{aligned} \quad (\text{C.15})$$

The third and fourth lines in eq. (C.15), which differ from the expressions in eq. (B.24), correspond to configurations in which one parton is emitted inside the jet cone while the other is emitted outside. For the uncorrelated double-real contribution, denoted by $C_i^2 h_{\text{in}} s_{\text{out}}$, the two pieces factorize according to the Non-Abelian Exponentiation (NAE) theorem. However, for correlated emissions, the presence of two distinct scales b_\perp and b^+ gives rise to NGLs in this configuration. Consequently, r_A and r_f acquire a nontrivial dependence on the ratio r , taking the form

$$r_A(r) = \frac{2\pi^2}{3\epsilon^2} + \left(-\frac{2}{3} + \frac{22\pi^2}{9} + 4\zeta_3 \right) \frac{1}{\epsilon} + C_{A,0}(r), \quad (\text{C.16})$$

$$r_f(r) = \frac{1}{\epsilon} \left(\frac{4}{3} - \frac{8\pi^2}{9} \right) + C_{f,0}(r), \quad (\text{C.17})$$

with r defined as

$$r = \frac{b_\perp R_j}{-b^+} = \frac{R}{2} \tan \phi_b. \quad (\text{C.18})$$

C.3 Refactorization of the hemisphere calculation and its power corrections

Eq. (B.24) and the hemisphere result in eq. (C.15) differ in their third and fourth lines, which encode the doubly correlated real-emission contribution with one emission inside the cone and the other outside. We now compare these terms after averaging over ϕ_b . After performing the ϕ_b average, the third line of eq. (B.24) becomes [51]

$$\left(\frac{\mu b_T}{b_0} \right)^{4\epsilon} \left[R^{-2\epsilon} C_i C_A \bar{p}_A + R^{-4\epsilon} (C_i C_A \bar{q}_A + C_i n_f T_F \bar{q}_f) \right], \quad (\text{C.19})$$

with $\bar{q}_A = q_A$, $\bar{q}_f = q_f$ and

$$\bar{p}_A = \frac{2\pi^2}{3\epsilon^2} + \left(8\zeta_3 - \frac{4}{3}\pi^2 \ln 2\right) \frac{1}{\epsilon} + \left(\frac{13\pi^4}{45} + \frac{4}{3}\pi^2 \ln^2 2 - 16\zeta_3 \ln 2\right). \quad (\text{C.20})$$

When comparing with the \bar{r}_f and \bar{r}_A in the ϕ_b -averaged boosted hemisphere soft functions eq. (B.24), we find that the following identities hold up to power corrections on the jet radius R ,

$$\begin{aligned} \bar{r}_A &= \bar{p}_A + R^{-2\epsilon} \bar{q}_A + \mathcal{O}(\epsilon^0 R \ln R, \epsilon^0 R) \\ &= \frac{2\pi^2}{3\epsilon^2} - \frac{2(3 - 11\pi^2 + 6\pi^2 \ln 2 - 18\zeta_3)}{9\epsilon} + \left[\left(\frac{4}{3} - \frac{44\pi^2}{9} + 8\zeta_3 \right) \ln R \right. \\ &\quad \left. + \frac{40}{9} + \frac{7\pi^4}{15} + \frac{\pi^2}{27} (-134 + 36 \ln^2 2) + \frac{44\zeta_3}{3} - 16\zeta_3 \ln 2 \right] + \mathcal{O}(\epsilon^0 R \ln R, \epsilon^0 R), \end{aligned} \quad (\text{C.21})$$

$$\begin{aligned} \bar{r}_f &= R^{-2\epsilon} \bar{q}_f + \mathcal{O}(\epsilon^0 R \ln R, \epsilon^0 R) \\ &= \left(\frac{4}{3} - \frac{8\pi^2}{9} \right) \frac{1}{\epsilon} + \frac{8}{9} (-3 + 2\pi^2) \ln R + \frac{4}{27} (-51 + 16\pi^2 - 36\zeta_3) + \mathcal{O}(\epsilon^0 R \ln R, \epsilon^0 R). \end{aligned} \quad (\text{C.22})$$

We compare the constant terms of \bar{r}_A (\bar{r}_f) with those of $\bar{p}_A + R^{-2\epsilon} \bar{q}_A$ ($R^{-2\epsilon} \bar{q}_f$) by plotting them, as shown in figure 9. The comparison demonstrates that the two approaches are consistent in the small radius limit $R \ll 1$. For finite jet radius, however, the hemisphere calculation contains power corrections on R relative to the multiplicity-interacting framework.

D Anomalous dimensions

The perturbative expansions of the cusp, non-cusp, and rapidity anomalous dimensions are

$$\gamma_{\text{cusp}} = \sum_{n=0}^{\infty} \left(\frac{\alpha_s}{4\pi} \right)^{n+1} \gamma_n^{\text{cusp}}, \quad \gamma_{\mu}^i = \sum_{n=0}^{\infty} \left(\frac{\alpha_s}{4\pi} \right)^{n+1} \gamma_n^i, \quad \gamma_{\nu}^i = \sum_{n=0}^{\infty} \left(\frac{\alpha_s}{4\pi} \right)^{n+1} \gamma_n^{\nu}. \quad (\text{D.1})$$

The cusp anomalous dimension, computed up to the three-loop order, is given by [106, 107]

$$\begin{aligned} \gamma_0^{\text{cusp}} &= 4, \\ \gamma_1^{\text{cusp}} &= \left(\frac{268}{9} - \frac{4\pi^2}{3} \right) C_A - \frac{80}{9} T_F n_f, \\ \gamma_2^{\text{cusp}} &= C_A^2 \left(\frac{490}{3} - \frac{536\pi^2}{27} + \frac{44\pi^4}{45} + \frac{88}{3} \zeta_3 \right) + C_A T_F n_f \left(-\frac{1672}{27} + \frac{160\pi^2}{27} - \frac{224}{3} \zeta_3 \right) \\ &\quad + C_F T_F n_f \left(-\frac{220}{3} + 64\zeta_3 \right) - \frac{64}{27} T_F^2 n_f^2. \end{aligned} \quad (\text{D.2})$$

The non-cusp anomalous dimensions for the hard function are derived from the massless quark and gluon form factors, which are known up to three-loop order [93, 108–110]. Explicitly, we list the results up to two loops necessary for NNLL resummation,

$$\gamma_0^q = -3C_F,$$

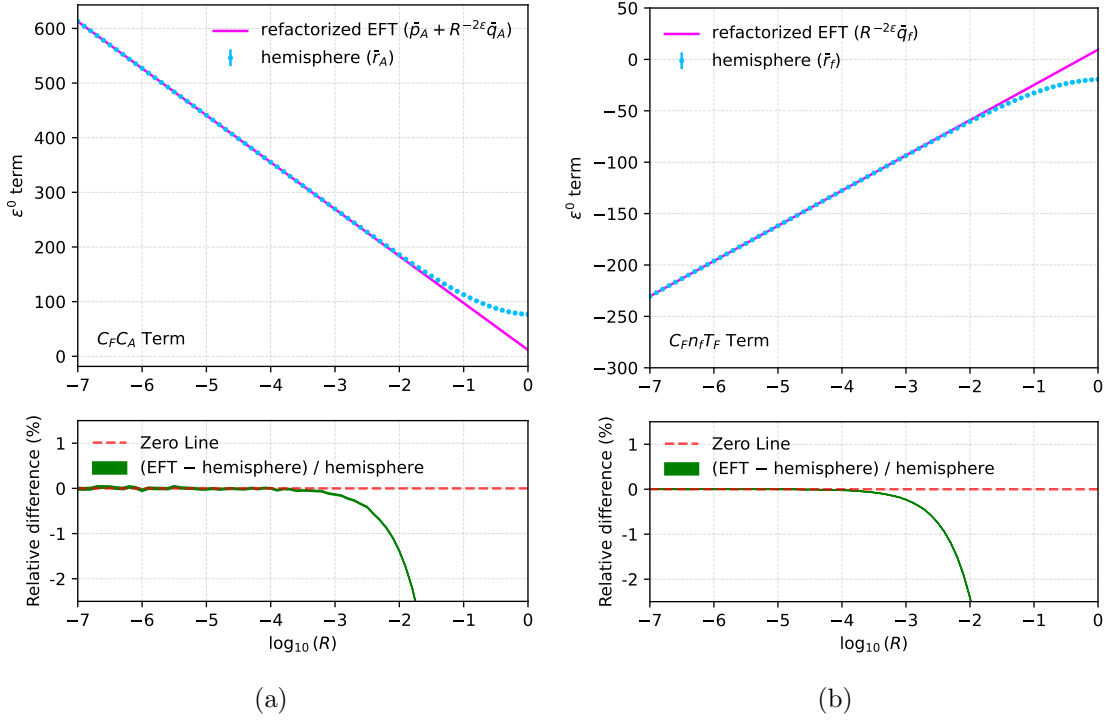


Figure 9: Comparison of the $\mathcal{O}(\epsilon^0)$ terms of the $C_F C_A$ and $C_F n_f T_F$ color structure for the hemisphere soft function with the corresponding refactorized expressions in the multi-Wilson-line EFT framework. Panel (a) compares \bar{r}_A against $\bar{p}_A + R^{-2\epsilon}\bar{q}_A$, while panel (b) compares \bar{r}_f against $R^{-2\epsilon}\bar{q}_f$, where $\bar{r}_{A,f}$ corresponds to the hemisphere soft function.

$$\begin{aligned}
\gamma_1^q &= C_F^2 \left(-\frac{3}{2} + 2\pi^2 - 24\zeta_3 \right) + C_F C_A \left(-\frac{961}{54} - \frac{11\pi^2}{6} + 26\zeta_3 \right) + C_F T_F n_f \left(\frac{130}{27} + \frac{2\pi^2}{3} \right), \\
\gamma_0^g &= -\beta_0 = -\frac{11}{3} C_A + \frac{4}{3} T_F n_f, \\
\gamma_1^g &= C_A^2 \left(-\frac{692}{27} + \frac{11\pi^2}{18} + 2\zeta_3 \right) + C_A T_F n_f \left(\frac{256}{27} - \frac{2\pi^2}{9} \right) + 4C_F T_F n_f, \tag{D.3}
\end{aligned}$$

The non-cusp anomalous dimensions for the beam functions and the WTA jet function are [102]

$$\begin{aligned}
\gamma_0^{Bq} &= \gamma_0^{Jq} = 6C_F, \\
\gamma_1^{bq} &= \gamma_1^{Jq} = C_F^2 (3 - 4\pi^2 + 48\zeta_3) + C_F C_A \left(\frac{17}{3} + \frac{44\pi^2}{9} - 24\zeta_3 \right) \\
&\quad + C_F T_F n_f \left(-\frac{4}{3} - \frac{16\pi^2}{9} \right), \\
\gamma_0^{Bg} &= \gamma_0^{Jg} = 2\beta_0, \\
\gamma_1^{Bg} &= \gamma_1^{Jg} = C_A^2 \left(\frac{64}{3} + 24\zeta_3 \right) - \frac{32}{3} C_A T_F n_f - 8C_F T_F n_f. \tag{D.4}
\end{aligned}$$

The non-cusp anomalous dimensions for the soft function read [111]

$$\gamma_0^S = 0, \quad \gamma_1^S = C_A \left(\frac{64}{9} - 28\zeta_3 \right) + \beta_0 \left(\frac{56}{9} - \frac{\pi^2}{3} \right). \quad (\text{D.5})$$

Finally, we present the non-cusp rapidity anomalous dimensions [102, 112–114],

$$\gamma_0^\nu = 0, \quad \gamma_1^\nu = -C_A \left(\frac{128}{9} - 56\zeta_3 \right) - \beta_0 \frac{112}{9}. \quad (\text{D.6})$$

References

- [1] CMS collaboration, *Event Shapes and Azimuthal Correlations in Z + Jets Events in pp Collisions at $\sqrt{s} = 7$ TeV*, *Phys. Lett.* **B722** (2013) 238 [[1301.1646](#)].
- [2] ATLAS collaboration, *High- E_T isolated-photon plus jets production in pp collisions at $\sqrt{s} = 8$ TeV with the ATLAS detector*, *Nucl. Phys. B* **918** (2017) 257 [[1611.06586](#)].
- [3] CMS collaboration, *Study of Jet Quenching with Z + jet Correlations in Pb-Pb and pp Collisions at $\sqrt{s_{NN}} = 5.02$ TeV*, *Phys. Rev. Lett.* **119** (2017) 082301 [[1702.01060](#)].
- [4] ATLAS collaboration, *Measurement of the cross section for isolated-photon plus jet production in pp collisions at $\sqrt{s} = 13$ TeV using the ATLAS detector*, *Phys. Lett.* **B780** (2018) 578 [[1801.00112](#)].
- [5] CMS collaboration, *Study of jet quenching with isolated-photon+jet correlations in PbPb and pp collisions at $\sqrt{s_{NN}} = 5.02$ TeV*, *Phys. Lett. B* **785** (2018) 14 [[1711.09738](#)].
- [6] ATLAS collaboration, *Measurement of Dijet Azimuthal Decorrelations in pp Collisions at $\sqrt{s} = 7$ TeV*, *Phys. Rev. Lett.* **106** (2011) 172002 [[1102.2696](#)].
- [7] CMS collaboration, *Dijet Azimuthal Decorrelations in pp Collisions at $\sqrt{s} = 7$ TeV*, *Phys. Rev. Lett.* **106** (2011) 122003 [[1101.5029](#)].
- [8] CMS collaboration, *Measurement of dijet azimuthal decorrelation in pp collisions at $\sqrt{s} = 8$ TeV*, *Eur. Phys. J. C* **76** (2016) 536 [[1602.04384](#)].
- [9] CMS collaboration, *Azimuthal correlations for inclusive 2-jet, 3-jet, and 4-jet events in pp collisions at $\sqrt{s} = 13$ TeV*, *Eur. Phys. J. C* **78** (2018) 566 [[1712.05471](#)].
- [10] ATLAS collaboration, *Measurement of dijet azimuthal decorrelations in pp collisions at $\sqrt{s} = 8$ TeV with the ATLAS detector and determination of the strong coupling*, *Phys. Rev. D* **98** (2018) 092004 [[1805.04691](#)].
- [11] CMS collaboration, *Azimuthal separation in nearly back-to-back jet topologies in inclusive 2- and 3-jet events in pp collisions at $\sqrt{s} = 13$ TeV*, *Eur. Phys. J. C* **79** (2019) 773 [[1902.04374](#)].
- [12] ATLAS collaboration, *Jet energy resolution in proton-proton collisions at $\sqrt{s} = 7$ TeV recorded in 2010 with the ATLAS detector*, *Eur. Phys. J. C* **73** (2013) 2306 [[1210.6210](#)].
- [13] CMS collaboration, *Determination of Jet Energy Calibration and Transverse Momentum Resolution in CMS*, *JINST* **6** (2011) P11002 [[1107.4277](#)].
- [14] D. Boer and W. Vogelsang, *Asymmetric jet correlations in p p uparrow scattering*, *Phys. Rev. D* **69** (2004) 094025 [[hep-ph/0312320](#)].

- [15] C.J. Bomhof, P.J. Mulders, W. Vogelsang and F. Yuan, *Single-Transverse Spin Asymmetry in Dijet Correlations at Hadron Colliders*, *Phys. Rev. D* **75** (2007) 074019 [[hep-ph/0701277](#)].
- [16] J.-W. Qiu, W. Vogelsang and F. Yuan, *Single Transverse-Spin Asymmetry in Hadronic Dijet Production*, *Phys. Rev. D* **76** (2007) 074029 [[0706.1196](#)].
- [17] W. Vogelsang and F. Yuan, *Hadronic Dijet Imbalance and Transverse-Momentum Dependent Parton Distributions*, *Phys. Rev. D* **76** (2007) 094013 [[0708.4398](#)].
- [18] Z.-B. Kang, K. Lee, D.Y. Shao and J. Terry, *The Sivers Asymmetry in Hadronic Dijet Production*, *JHEP* **02** (2021) 066 [[2008.05470](#)].
- [19] X. Liu, F. Ringer, W. Vogelsang and F. Yuan, *Factorization and its Breaking in Dijet Single Transverse Spin Asymmetries in pp Collisions*, *Phys. Rev. D* **102** (2020) 114012 [[2008.03666](#)].
- [20] STAR collaboration, *Measurement of transverse single-spin asymmetries for dijet production in polarized proton-proton collisions at $\sqrt{s} = 200$ GeV*, [2305.10359](#).
- [21] J. Collins and J.-W. Qiu, *k_T factorization is violated in production of high-transverse-momentum particles in hadron-hadron collisions*, *Phys. Rev. D* **75** (2007) 114014 [[0705.2141](#)].
- [22] T.C. Rogers and P.J. Mulders, *No Generalized TMD-Factorization in Hadro-Production of High Transverse Momentum Hadrons*, *Phys. Rev. D* **81** (2010) 094006 [[1001.2977](#)].
- [23] J.R. Gaunt, *Glauber Gluons and Multiple Parton Interactions*, *JHEP* **07** (2014) 110 [[1405.2080](#)].
- [24] M. Zeng, *Drell-Yan process with jet vetoes: breaking of generalized factorization*, *JHEP* **10** (2015) 189 [[1507.01652](#)].
- [25] S. Catani, D. de Florian and G. Rodrigo, *Space-like (versus time-like) collinear limits in QCD: Is factorization violated?*, *JHEP* **07** (2012) 026 [[1112.4405](#)].
- [26] J.R. Forshaw, M.H. Seymour and A. Siodmok, *On the Breaking of Collinear Factorization in QCD*, *JHEP* **11** (2012) 066 [[1206.6363](#)].
- [27] M.D. Schwartz, K. Yan and H.X. Zhu, *Collinear factorization violation and effective field theory*, *Phys. Rev. D* **96** (2017) 056005 [[1703.08572](#)].
- [28] L. Cieri, P.K. Dhani and G. Rodrigo, *Catani's generalization of collinear factorization breaking*, [2402.14749](#).
- [29] J. Henn, R. Ma, Y. Xu, K. Yan, Y. Zhang and H.X. Zhu, *Two-loop spacelike splitting amplitude for $N=4$ Super-Yang-Mills theory*, *Phys. Rev. D* **112** (2025) 076003 [[2406.14604](#)].
- [30] X. Guan, F. Herzog, Y. Ma, B. Mistlberger and A. Suresh, *Splitting amplitudes at N^3 LO in QCD*, *JHEP* **01** (2025) 090 [[2408.03019](#)].
- [31] M. Dasgupta and G.P. Salam, *Resummation of nonglobal QCD observables*, *Phys. Lett.* **B512** (2001) 323 [[hep-ph/0104277](#)].
- [32] Y. Hatta and T. Ueda, *Resummation of non-global logarithms at finite N_c* , *Nucl. Phys.* **B874** (2013) 808 [[1304.6930](#)].
- [33] A.J. Larkoski, I. Moult and D. Neill, *Non-Global Logarithms, Factorization, and the Soft Substructure of Jets*, *JHEP* **09** (2015) 143 [[1501.04596](#)].

- [34] S. Caron-Huot, *Resummation of non-global logarithms and the BFKL equation*, *JHEP* **03** (2018) 036 [[1501.03754](#)].
- [35] T. Becher, M. Neubert, L. Rothen and D.Y. Shao, *Effective Field Theory for Jet Processes*, *Phys. Rev. Lett.* **116** (2016) 192001 [[1508.06645](#)].
- [36] T. Becher, M. Neubert, L. Rothen and D.Y. Shao, *Factorization and Resummation for Jet Processes*, *JHEP* **11** (2016) 019 [[1605.02737](#)].
- [37] P. Sun, C.P. Yuan and F. Yuan, *Soft Gluon Resummations in Dijet Azimuthal Angular Correlations in Hadronic Collisions*, *Phys. Rev. Lett.* **113** (2014) 232001 [[1405.1105](#)].
- [38] P. Sun, C.P. Yuan and F. Yuan, *Transverse Momentum Resummation for Dijet Correlation in Hadronic Collisions*, *Phys. Rev.* **D92** (2015) 094007 [[1506.06170](#)].
- [39] X. Liu, F. Ringer, W. Vogelsang and F. Yuan, *Lepton-jet Correlations in Deep Inelastic Scattering at the Electron-Ion Collider*, *Phys. Rev. Lett.* **122** (2019) 192003 [[1812.08077](#)].
- [40] Y.-T. Chien, D.Y. Shao and B. Wu, *Resummation of Boson-Jet Correlation at Hadron Colliders*, *JHEP* **11** (2019) 025 [[1905.01335](#)].
- [41] M.-S. Gao, Z.-B. Kang, D.Y. Shao, J. Terry and C. Zhang, *QCD resummation of dijet azimuthal decorrelations in pp and pA collisions*, *JHEP* **10** (2023) 013 [[2306.09317](#)].
- [42] M. Balsiger, T. Becher and D.Y. Shao, *NLL' resummation of jet mass*, *JHEP* **04** (2019) 020 [[1901.09038](#)].
- [43] A. Banfi, F.A. Dreyer and P.F. Monni, *Next-to-leading non-global logarithms in QCD*, *JHEP* **10** (2021) 006 [[2104.06416](#)].
- [44] T. Becher, N. Schalch and X. Xu, *Resummation of Next-to-Leading Nonglobal Logarithms at the LHC*, *Phys. Rev. Lett.* **132** (2024) 081602 [[2307.02283](#)].
- [45] G. Salam, “ E_t^∞ Scheme.” Unpublished.
- [46] D. Bertolini, T. Chan and J. Thaler, *Jet Observables Without Jet Algorithms*, *JHEP* **04** (2014) 013 [[1310.7584](#)].
- [47] A. Banfi, M. Dasgupta and Y. Delenda, *Azimuthal decorrelations between QCD jets at all orders*, *Phys. Lett. B* **665** (2008) 86 [[0804.3786](#)].
- [48] A.J. Larkoski, D. Neill and J. Thaler, *Jet Shapes with the Broadening Axis*, *JHEP* **04** (2014) 017 [[1401.2158](#)].
- [49] Y.-T. Chien, R. Rahn, S. Schrijnder van Velzen, D.Y. Shao, W.J. Waalewijn and B. Wu, *Recoil-free azimuthal angle for precision boson-jet correlation*, *Phys. Lett. B* **815** (2021) 136124 [[2005.12279](#)].
- [50] Y.-T. Chien, R. Rahn, D.Y. Shao, W.J. Waalewijn and B. Wu, *Precision boson-jet azimuthal decorrelation at hadron colliders*, *JHEP* **02** (2023) 256 [[2205.05104](#)].
- [51] R.-J. Fu, R. Rahn, D.Y. Shao, W.J. Waalewijn and B. Wu, *qT Slicing with Multiple Jets*, *Phys. Rev. Lett.* **135** (2025) 17 [[2412.05358](#)].
- [52] C.W. Bauer, S. Fleming and M.E. Luke, *Summing Sudakov logarithms in $B \rightarrow X_s \gamma$ in effective field theory*, *Phys. Rev.* **D63** (2000) 014006 [[hep-ph/0005275](#)].
- [53] C.W. Bauer, S. Fleming, D. Pirjol and I.W. Stewart, *An Effective field theory for collinear and soft gluons: Heavy to light decays*, *Phys. Rev.* **D63** (2001) 114020 [[hep-ph/0011336](#)].

- [54] C.W. Bauer and I.W. Stewart, *Invariant operators in collinear effective theory*, *Phys. Lett.* **B516** (2001) 134 [[hep-ph/0107001](#)].
- [55] C.W. Bauer, D. Pirjol and I.W. Stewart, *Soft collinear factorization in effective field theory*, *Phys. Rev.* **D65** (2002) 054022 [[hep-ph/0109045](#)].
- [56] C.W. Bauer, S. Fleming, D. Pirjol, I.Z. Rothstein and I.W. Stewart, *Hard scattering factorization from effective field theory*, *Phys. Rev.* **D66** (2002) 014017 [[hep-ph/0202088](#)].
- [57] M. Beneke, A.P. Chapovsky, M. Diehl and T. Feldmann, *Soft collinear effective theory and heavy to light currents beyond leading power*, *Nucl. Phys.* **B643** (2002) 431 [[hep-ph/0206152](#)].
- [58] M. Rubin, G.P. Salam and S. Sapeta, *Giant QCD K-factors beyond NLO*, *JHEP* **09** (2010) 084 [[1006.2144](#)].
- [59] Z. Nagy and Z. Trocsanyi, *Multijet cross-sections in deep inelastic scattering at next-to-leading order*, *Phys. Rev. Lett.* **87** (2001) 082001 [[hep-ph/0104315](#)].
- [60] Z. Nagy, *Three jet cross-sections in hadron hadron collisions at next-to-leading order*, *Phys. Rev. Lett.* **88** (2002) 122003 [[hep-ph/0110315](#)].
- [61] Z. Nagy, *Next-to-leading order calculation of three jet observables in hadron hadron collision*, *Phys. Rev. D* **68** (2003) 094002 [[hep-ph/0307268](#)].
- [62] M. Cacciari, G.P. Salam and G. Soyez, *FastJet User Manual*, *Eur. Phys. J. C* **72** (2012) 1896 [[1111.6097](#)].
- [63] C. Bierlich et al., *A comprehensive guide to the physics and usage of PYTHIA 8.3*, *SciPost Phys. Codeb.* **2022** (2022) 8 [[2203.11601](#)].
- [64] J.C. Collins and D.E. Soper, *Back-To-Back Jets in QCD*, *Nucl. Phys.* **B193** (1981) 381.
- [65] J.C. Collins, D.E. Soper and G.F. Sterman, *Transverse Momentum Distribution in Drell-Yan Pair and W and Z Boson Production*, *Nucl. Phys.* **B250** (1985) 199.
- [66] T. Becher and M. Neubert, *Drell-Yan Production at Small q_T , Transverse Parton Distributions and the Collinear Anomaly*, *Eur. Phys. J. C* **71** (2011) 1665 [[1007.4005](#)].
- [67] T. Becher, M. Neubert and D. Wilhelm, *Electroweak Gauge-Boson Production at Small q_T : Infrared Safety from the Collinear Anomaly*, *JHEP* **02** (2012) 124 [[1109.6027](#)].
- [68] J.-y. Chiu, A. Jain, D. Neill and I.Z. Rothstein, *The Rapidity Renormalization Group*, *Phys. Rev. Lett.* **108** (2012) 151601 [[1104.0881](#)].
- [69] J.-Y. Chiu, A. Jain, D. Neill and I.Z. Rothstein, *A Formalism for the Systematic Treatment of Rapidity Logarithms in Quantum Field Theory*, *JHEP* **05** (2012) 084 [[1202.0814](#)].
- [70] A. Broggio, A. Ferroglia, B.D. Pecjak and Z. Zhang, *NNLO hard functions in massless QCD*, *JHEP* **12** (2014) 005 [[1409.5294](#)].
- [71] J.C. Collins and D.E. Soper, *Parton Distribution and Decay Functions*, *Nucl. Phys.* **B194** (1982) 445.
- [72] M.-x. Luo, T.-Z. Yang, H.X. Zhu and Y.J. Zhu, *Quark Transverse Parton Distribution at the Next-to-Next-to-Next-to-Leading Order*, *Phys. Rev. Lett.* **124** (2020) 092001 [[1912.05778](#)].
- [73] A. Behring, K. Melnikov, R. Rietkerk, L. Tancredi and C. Wever, *Quark beam function at*

next-to-next-to-next-to-leading order in perturbative QCD in the generalized large- N_c approximation, *Phys. Rev. D* **100** (2019) 114034 [[1910.10059](#)].

- [74] M.A. Ebert, B. Mistlberger and G. Vita, *Transverse momentum dependent PDFs at N^3LO* , *JHEP* **09** (2020) 146 [[2006.05329](#)].
- [75] D. Gutierrez-Reyes, S. Leal-Gomez, I. Scimemi and A. Vladimirov, *Linearly polarized gluons at next-to-next-to leading order and the Higgs transverse momentum distribution*, *JHEP* **11** (2019) 121 [[1907.03780](#)].
- [76] D. Gutierrez-Reyes, I. Scimemi, W.J. Waalewijn and L. Zoppi, *Transverse momentum dependent distributions with jets*, *Phys. Rev. Lett.* **121** (2018) 162001 [[1807.07573](#)].
- [77] D. Gutierrez-Reyes, I. Scimemi, W.J. Waalewijn and L. Zoppi, *Transverse momentum dependent distributions in e^+e^- and semi-inclusive deep-inelastic scattering using jets*, *JHEP* **10** (2019) 031 [[1904.04259](#)].
- [78] T. Becher and M. Neubert, *Infrared singularities of scattering amplitudes in perturbative QCD*, *Phys. Rev. Lett.* **102** (2009) 162001 [[0901.0722](#)].
- [79] S. Catani and M.H. Seymour, *A General algorithm for calculating jet cross-sections in NLO QCD*, *Nucl. Phys. B* **485** (1997) 291 [[hep-ph/9605323](#)].
- [80] N. Kidonakis, G. Oderda and G.F. Sterman, *Evolution of color exchange in QCD hard scattering*, *Nucl. Phys. B* **531** (1998) 365 [[hep-ph/9803241](#)].
- [81] N. Kidonakis, G. Oderda and G.F. Sterman, *Threshold resummation for dijet cross-sections*, *Nucl. Phys. B* **525** (1998) 299 [[hep-ph/9801268](#)].
- [82] S.M. Aybat, L.J. Dixon and G.F. Sterman, *The Two-loop soft anomalous dimension matrix and resummation at next-to-next-to leading pole*, *Phys. Rev. D* **74** (2006) 074004 [[hep-ph/0607309](#)].
- [83] S.M. Aybat, L.J. Dixon and G.F. Sterman, *The Two-loop anomalous dimension matrix for soft gluon exchange*, *Phys. Rev. Lett.* **97** (2006) 072001 [[hep-ph/0606254](#)].
- [84] A. Gao, H.T. Li, I. Moutl and H.X. Zhu, *The transverse energy-energy correlator at next-to-next-to-next-to-leading logarithm*, *JHEP* **09** (2024) 072 [[2312.16408](#)].
- [85] T. Becher, B.D. Pecjak and D.Y. Shao, *Factorization for the light-jet mass and hemisphere soft function*, *JHEP* **12** (2016) 018 [[1610.01608](#)].
- [86] S. Catani and M.H. Seymour, *The Dipole formalism for the calculation of QCD jet cross-sections at next-to-leading order*, *Phys. Lett. B* **378** (1996) 287 [[hep-ph/9602277](#)].
- [87] F. Landry, R. Brock, P.M. Nadolsky and C.P. Yuan, *Tevatron Run-1 Z boson data and Collins-Soper-Sterman resummation formalism*, *Phys. Rev. D* **67** (2003) 073016 [[hep-ph/0212159](#)].
- [88] A.V. Konychev and P.M. Nadolsky, *Universality of the Collins-Soper-Sterman nonperturbative function in gauge boson production*, *Phys. Lett. B* **633** (2006) 710 [[hep-ph/0506225](#)].
- [89] J. Collins and T. Rogers, *Understanding the large-distance behavior of transverse-momentum-dependent parton densities and the Collins-Soper evolution kernel*, *Phys. Rev. D* **91** (2015) 074020 [[1412.3820](#)].
- [90] C.A. Aidala, B. Field, L.P. Gamberg and T.C. Rogers, *Limits on transverse momentum*

dependent evolution from semi-inclusive deep inelastic scattering at moderate Q , *Phys. Rev. D* **89** (2014) 094002 [[1401.2654](#)].

- [91] P. Sun, J. Isaacson, C.P. Yuan and F. Yuan, *Nonperturbative functions for SIDIS and Drell–Yan processes*, *Int. J. Mod. Phys. A* **33** (2018) 1841006 [[1406.3073](#)].
- [92] M. Dasgupta, K. Khelifa-Kerfa, S. Marzani and M. Spannowsky, *On jet mass distributions in Z +jet and dijet processes at the LHC*, *JHEP* **10** (2012) 126 [[1207.1640](#)].
- [93] T. Becher, M. Neubert and B.D. Pecjak, *Factorization and Momentum-Space Resummation in Deep-Inelastic Scattering*, *JHEP* **01** (2007) 076 [[hep-ph/0607228](#)].
- [94] M. Cacciari, G.P. Salam and G. Soyez, *The anti- k_t jet clustering algorithm*, *JHEP* **04** (2008) 063 [[0802.1189](#)].
- [95] M.A. Ebert and F.J. Tackmann, *Impact of isolation and fiducial cuts on q_T and N -jettiness subtractions*, *JHEP* **03** (2020) 158 [[1911.08486](#)].
- [96] G.P. Salam and E. Slade, *Cuts for two-body decays at colliders*, *JHEP* **11** (2021) 220 [[2106.08329](#)].
- [97] M. Grazzini, S. Kallweit and M. Wiesemann, *Fully differential NNLO computations with MATRIX*, *Eur. Phys. J. C* **78** (2018) 537 [[1711.06631](#)].
- [98] S. Alekhin, A. Kardos, S. Moch and Z. Trócsányi, *Precision studies for Drell–Yan processes at NNLO*, *Eur. Phys. J. C* **81** (2021) 573 [[2104.02400](#)].
- [99] X. Chen, Y. Dai, H.T. Li, S.-Y. Li, H.-S. Shao and J. Wang, *Fully differential Higgs boson pair production at N^3 LO with top quark mass effects*, [2601.19990](#).
- [100] M.A. Ebert, I. Moulst, I.W. Stewart, F.J. Tackmann, G. Vita and H.X. Zhu, *Subleading power rapidity divergences and power corrections for q_T* , *JHEP* **04** (2019) 123 [[1812.08189](#)].
- [101] T. Becher and T. Neumann, *Fiducial q_T resummation of color-singlet processes at N^3 LL+NNLO*, *JHEP* **03** (2021) 199 [[2009.11437](#)].
- [102] T. Lübbert, J. Oredsson and M. Stahlhofen, *Rapidity renormalized TMD soft and beam functions at two loops*, *JHEP* **03** (2016) 168 [[1602.01829](#)].
- [103] R.F. del Castillo, M.G. Echevarria, Y. Makris and I. Scimemi, *TMD factorization for dijet and heavy-meson pair in DIS*, *JHEP* **01** (2021) 088 [[2008.07531](#)].
- [104] G. Bell, R. Rahn and J. Talbert, *Generic dijet soft functions at two-loop order: correlated emissions*, *JHEP* **07** (2019) 101 [[1812.08690](#)].
- [105] R. Kelley, M.D. Schwartz, R.M. Schabinger and H.X. Zhu, *The two-loop hemisphere soft function*, *Phys. Rev. D* **84** (2011) 045022 [[1105.3676](#)].
- [106] G.P. Korchemsky and A.V. Radyushkin, *Renormalization of the Wilson Loops Beyond the Leading Order*, *Nucl. Phys. B* **283** (1987) 342.
- [107] S. Moch, J.A.M. Vermaseren and A. Vogt, *The Three loop splitting functions in QCD: The Nonsinglet case*, *Nucl. Phys. B* **688** (2004) 101 [[hep-ph/0403192](#)].
- [108] A. Idilbi, X.-d. Ji and F. Yuan, *Resummation of threshold logarithms in effective field theory for DIS, Drell–Yan and Higgs production*, *Nucl. Phys. B* **753** (2006) 42 [[hep-ph/0605068](#)].
- [109] T. Becher and M. Neubert, *On the Structure of Infrared Singularities of Gauge-Theory Amplitudes*, *JHEP* **06** (2009) 081 [[0903.1126](#)].

- [110] S. Moch, J.A.M. Vermaseren and A. Vogt, *Three-loop results for quark and gluon form-factors*, *Phys. Lett. B* **625** (2005) 245 [[hep-ph/0508055](#)].
- [111] Y. Li, A. von Manteuffel, R.M. Schabinger and H.X. Zhu, *Soft-virtual corrections to Higgs production at N^3LO* , *Phys. Rev. D* **91** (2015) 036008 [[1412.2771](#)].
- [112] T. Gehrmann, T. Lubbert and L.L. Yang, *Transverse parton distribution functions at next-to-next-to-leading order: the quark-to-quark case*, *Phys. Rev. Lett.* **109** (2012) 242003 [[1209.0682](#)].
- [113] T. Gehrmann, T. Luebbert and L.L. Yang, *Calculation of the transverse parton distribution functions at next-to-next-to-leading order*, *JHEP* **06** (2014) 155 [[1403.6451](#)].
- [114] M.G. Echevarria, I. Scimemi and A. Vladimirov, *Universal transverse momentum dependent soft function at NNLO*, *Phys. Rev. D* **93** (2016) 054004 [[1511.05590](#)].